

## The Radial Integral of the Geopotential

Robert Tenzer<sup>1</sup> · Pavel Novák<sup>2</sup> · Mehdi Eshagh<sup>3</sup>

Received: 23 November 2024 / Accepted: 21 May 2025 / Published online: 30 June 2025 © The Author(s) 2025

#### Abstract

In Newtonian theory of gravitation, used in Earth's and planetary sciences, gravitational acceleration is standardly regarded as the most fundamental parameter that describes any vectorial gravitational field. Considering only conservative gravitational field, the vectorial field can be described by a scalar function of 3D position called gravitational potential from which other parameters (particularly gravitational acceleration and gravitational gradient) are derived by applying gradient operators. Gradients of the Earth's gravity potential are nowadays measured with high accuracy and applied in various geodetic and geophysical applications. In geodesy, the gravity and gravity gradient measurements are used to determine the Earth's gravity potential (i.e., the geopotential) that is related to geometry of equipotential surfaces, most notably the geoid approximating globally the mean sea surface. Reversely to the application of gradient operator, the application of radial integral to gravity yields the gravity potential differences and the same application to gravity gradient yields the gravity differences. This procedure was implemented in definitions of rigorous orthometric heights and differences between normal and orthometric heights (i.e., the geoid-to-quasigeoid separation). Following this concept, we introduce the radially integrated geopotential, and provide its mathematical definitions in spatial and spectral domains. We also define its relationship with other parameters of the Earth's gravity field via Poisson, Hotine, and Stokes integrals. In numerical studies, we investigate a spatial pattern and spectrum of the radial integral of the disturbing potential (i.e., difference between actual and normal gravity potentials) and compare them with other parameters of gravity field. We demonstrate that the application of radial integral operator smooths a spatial pattern of the disturbing potential. This finding is explained by the fact that more detailed features in the disturbing potential (mainly attributed to a gravitational signature of lithospheric density structure and geometry) are filtered out proportionally with increasing degree of spherical harmonics in this functional. In the global geoidal geometry (and the disturbing potential), on the other hand, the gravitational signature of lithosphere is still clearly manifested—most notably across large orogens—even after applying either spectral decompensation or filtering.

**Keywords** Geopotential · Radial integral of the geopotential · Spherical harmonics · Mantle





#### **Article Highlights**

- We conceptualize the definition of the radial integral of the geopotential
- We derive functional relationships between this quantity and other parameters of the Earth's gravity field via Hotine, and Stokes integrals
- We demonstrate that application of the radial integral operator smooths a spatial pattern
  of the disturbing potential.

#### 1 Introduction

Gravitational acceleration is the most fundamental parameter describing the vectorial gravitational field. Assuming its conservative form (adopting some simplifications in case of the real Earth), it can be described by the scalar function of 3D position called gravitational potential. Due to the Earth's rotation, the superposition of the centrifugal and gravitational potentials results in the Earth's gravity potential (i.e., the geopotential). The static geopotential is a scalar function of 3D position of which unit is m² s<sup>-2</sup>. The geopotential plays a crucial role in defining geometry of equipotential surfaces of the Earth's gravity field. In 1828, Gauss postulated the concept of representing the physical figure of the Earth by the geoid. According to his definition, the geoid is the equipotential surface of the static Earth's gravity field that best fits (in the least-squares sense) the global mean sea level extended under the continents. The geoid constitutes the height reference (zero-height) surface for defining physical heights over the continents used in geodesy and surveying. The accurately determined marine geoid model is, on the other hand, crucial in studies of ocean dynamics and sea level changes.

The geopotential cannot be measured by classical methods used in physics, but its differences can be observed by atomic clocks based on adopting the relativistic theory of time dilatation (cf. Bjerhammar 1975; Vermeer 1983). A mathematical concept of deriving values of the geopotential from surface gravity measurements was postulated by Stokes (1849), and later discussed in detail by Helmert (1880) in his treatise on physical geodesy. The gravitational acceleration is a vector quantity that describes the acceleration excited by an attracting body, and its unit is m s<sup>-2</sup>. The Earth's gravity acceleration (magnitude of the vector or its components) is conventionally measured by gravimeters on and above the Earth's surface. In addition to gravity measurements, gravity gradient observations have been conducted (e.g., Meissl 1971), especially after launching the gravity field and steadystate ocean circulation explorer (GOCE) satellite gravity gradiometry mission (Drinkwater et al. 2003; Floberghagen et al. 2011). The gravity gradient describes change of the gravity acceleration in a particular direction. In 3D space, gradients form a 3×3 gradiometric tensor with unit in s<sup>-2</sup>. Out of its 9 components, 6 are unique (tensor is symmetric) and in mass-free space, only 5 components are independent. It is worth noting that theoretical studies have been published on gravity curvatures (i.e., geopotential gradients of the 3rd order) that define directional changes of gravity gradients (Sprlák and Novák, 2015; 2016; 2017), and their possible applications in geodesy and geophysics have been inspected in recent theoretical studies (e.g., Ji et al. 2023).

Various parameters of the static gravity field are functionally linked by means of applying the gradient operators. The gravity acceleration vector is defined as the first-order geopotential gradient, and the gravity gradient is defined as the gradient of the gravity acceleration vector (i.e., the second-order geopotential gradient tensor). These gravity field parameters and their functional relations were formulated and examined in



studies by Meissl (1971), Rummel and Van Gelderen (1992), Grafarend (2001), Heck (1991; 1997), Martinec (1998; 2003), and references therein. Reversely, the geopotential difference in a certain direction can be defined in terms of the line integral of the gravity acceleration, and the gravity acceleration difference in terms of the line integral of the gravity gradient. These functions were already applied in physical geodesy. Vaníček et al. (2001), for instance, defined the mean vertical gravity gradient within topographic masses as the difference of gravity values at the geoid and topographic surface. The integral mean of gravity along the plumbline within topographic masses, defined by means of the gravity potential differences of values computed at the geoid and topographic surface, was used in the rigorous definition of orthometric heights by Tenzer et al. (2005), and later incorporated for an accurate determination of the geoid-to-quasigeoid separation by Tenzer et al. (2006) and Sjöberg (2006).

For several decades, a significant effort has been dedicated to establish the world height system (e.g., Colombo 1980; Burša et al. 1999). Bjerhammar (1985; 1986) proposed the idea of using atomic clocks to measure the geopotential differences in his work on relativistic geodesy, while practical aspects of using these measurements for a vertical datum unification were investigated among others by Mai (2013), Kopeikin et al. (2018), Mehlstäubler et al. (2018), Puetzfeld et al., (2019), and Shen et al. (2011; 2019).

Along with the application of geopotential differences measured by atomic clocks for a vertical datum unification, these observations could also be used for the accuracy assessment of vertical geodetic controls practically realized by precise leveling and gravity measurements along leveling lines, particularly inspecting a possible presence of cumulative systematic errors in leveling measurements. Other applications can be identified based on defining functional relations between the geopotential differences and the geopotential, gravity, and gravity gradient values at the geoid (Tenzer et al. 2005). Since the geopotential differences could be used to compute the geopotential values at different heights with respect to the known reference geopotential, such as the geoidal geopotential value  $W_0$ , the radial integral of the geopotential might also offer possibilities for its practical applications. Moreover, this function could be linked with other parameters of the Earth's gravity field in a similar way to the geopotential differences.

In this study, we conceptualize the definition of the radial integral of the geopotential and inspect the possibility of applying this function in gravimetric geophysics in the context of interpreting the Earth's inner structure. The study is organized into four sections. Fundamental definitions of the radial integral of the geopotential are postulated in Sect. 2. Expressions defining functional relations between the radial integral of the geopotential and other parameters of the Earth's gravity field are derived in Sect. 3. Numerical results are presented and discussed in Sect. 4. Theoretical and numerical findings are summarized, and the study is concluded in Sect. 5.

## 2 Theory

In this section, we introduce the concept of the radial integral of the geopotential and summarize its computational formulas in spatial and spectral domains. As the centrifugal acceleration vector (and respective potential) can easily be computed for a given geocentric position, the focus is on the gravitational field and its parameters.



#### 2.1 Radial Integral of the Gravitational Potential

The gravitational acceleration vector  $\mathbf{g}$  is functionally related to the conservative gravitational potential V by applying the gradient operator in a point positioned by the geocentric vector  $\mathbf{x}$ , i.e.,  $\mathbf{g}(\mathbf{x}) = -\nabla V(\mathbf{x})$ , where the sign convention reflects the attenuation of the gravitational field with the increasing distance from gravitating masses. The gravitational potential difference  $\Delta V$  can be evaluated as a line integral of the gravitational attraction  $\mathbf{g}$  in the form of  $\Delta V = -\int \mathbf{g} \cdot d\mathbf{x}$ , where  $d\mathbf{x} = \mathbf{t} \, d\mathbf{s}$  denotes a product of the unit tangent vector  $\mathbf{t}$  and the infinitesimal length the line segment  $d\mathbf{s}$  (i.e., infinitesimal displacement vector); the dot operator represents a scalar product of two vectors. For the trajectory  $\mathcal{S}$  with two end points A and B, the potential difference  $\Delta V$  becomes  $V(x_B) - V(x_A) = -\int_{\mathcal{S}} \mathbf{g}(\mathbf{x}) \cdot \mathbf{t} \, d\mathbf{s}$ .

By analogy with the gravitational potential difference  $\Delta V$ , we define the line integral of the gravitational potential along the trajectory S as follows:

$$\mathfrak{F}(x_B) - \mathfrak{F}(x_A) = \int_{\mathcal{S}} V(x) ds$$
 (1)

where  $\mathfrak{F}$  is an indefinite integral function of the gravitational potential V in  $m^3$  s<sup>-2</sup>.

Since the largest geopotential gradient is along a plumbline normal to all equipotential surfaces, the line integral in Eq. (1) can be defined along the plumbline. Adopting the Earth's spherical approximation, i.e., in the spherical coordinates the gravitational potential function V depends only on the geocentric radius r (disregarding small geopotential changes due to approximating the plumbline by the radial direction). The line integral in Eq. (1) then becomes

$$\mathfrak{F}(r_2) - \mathfrak{F}(r_1) = \int_{r_1}^{r_2} V(r) dr$$
 (2)

where  $r_1$  and  $r_2$  represent the lower and upper integration limits, respectively.

To find the primitive function  $\mathfrak{F}$  for the radial integral of the gravitational potential in Eq. (2), we assume that the Earth is approximated by a radially symmetric mass density sphere of which the gravitational potential is simply defined as V(r) = GM/r, where GM denotes the geocentric gravitational constant.

Inserting V(r) = GM/r to the indefinite radial integral of the gravitational potential in Eq. (2), we get

$$\mathfrak{F}(r) = \int V(r) dr = \int \frac{GM}{r} dr = GM \int r^{-1} dr$$
 (3)

The radial integral of  $r^{-1}$  reads

$$\int r^{-1} dr = \ln|r| + C \tag{4}$$

where C is the integration constant.

Combining Eqs. (3) and (4), we arrive at

$$\mathfrak{F}(r) = GM (\ln r + C) \tag{5}$$

As seen in Eq. (5), the primitive function  $\mathfrak F$  of the radial integral of the gravitational potential V is a function of GM multiplied by the natural logarithm of r, as for  $r \ge 0$ ,  $\ln |r| = \ln r$ .



Substitution from Eq. (5) back to Eq. (2) yields

$$\mathfrak{F}(r_2) - \mathfrak{F}(r_1) = \int_{r_1}^{r_2} V dr = GM \ln r|_{r_1}^{r_2} = GM \left( \ln r_2 - \ln r_1 \right) = GM \ln \frac{r_2}{r_1}$$
 (6)

for  $r_1 \ge R$  and  $r_1 < r_2$ , where  $R = 6371 \times 10^3$  m denotes the mean Earth's radius. The solution of the radial integral of the potential in Eq. (6) is defined for the external gravitational field of the Earth that is approximated by the mean geocentric sphere with the radius R. The unit of  $\mathfrak{F}$  is m<sup>3</sup> s<sup>-2</sup>. Note that the radial integral of the gravitational potential has the same unit (dimension) as the geocentric gravitational constant GM. It is also worth noting that the application of gradient operator to this function yields gravitational potential, i.e.,  $\nabla \mathfrak{F} = \frac{\partial \mathfrak{F}}{\partial r} = GM \frac{\partial}{\partial r} \ln r = GM r^{-1} = V$ .

#### 2.2 Radial Integral of the Earth's Gravitational Potential

We further extend the definition of the radial integral of the gravitational potential *V* generated by the Earth. Assuming again the spherical Earth, the Earth's gravitational potential *V* is defined by Newton's volume integral in the following form (Kellogg 1967):

$$V = V(r, \Omega) = G \int \int_{0}^{R+H'} \rho(r', \Omega') \mathcal{E}^{-1}(r, \psi, r') r'^2 dr' d\Omega'$$
 (7)

The gravitational potential V in Eq. (7) is defined for the external computation point  $(r, \Omega)$ , i.e.,  $V(r, \Omega)$ ; where r is the geocentric radius, the pair  $\Omega = (\theta, \lambda)$  represents the geocentric direction of the computation point with  $\theta$  and  $\lambda$  denoting spherical co-latitude and longitude, respectively.

The volume integral on the right-hand side of Eq. (7) is evaluated for the 3D mass density distribution function  $\rho(r',\Omega')$  within the Earth's interior limited by the Earth's surface described by the geocentric radius r' = R + H' that is defined approximately as the mean Earth's radius R plus the topographic height function H with  $H' = H(\Omega')$ . The term  $d\Omega' = \sin\theta' d\theta' d\lambda'$  denotes an infinitesimal surface element of a unit sphere,  $\{\Omega' = (\theta', \lambda') : \theta' \in [0, \pi] \land \lambda' \in [0, 2\pi)\}$  represents the full spatial angle, and  $\int d\Omega' = \iint \sin\theta' d\theta' d\lambda'$ .

The Euclidean spatial distance  $\ell$  between the computation and integration (running) points in Eq. (7) reads

$$\ell(r, \psi, r') = \sqrt{r^2 + r'^2 - 2rr'\cos\psi} \tag{8}$$

where  $\cos \psi = \cos \theta \cos \theta t + \sin \theta \sin \theta t \cos(\lambda t - \lambda)$  is cosine of the spherical distance  $\psi$  between the two points.

By analogy with Eq. (3), we define the radial integral of the Earth's gravitational potential V, see Eq. (7), as follows:

$$\int V dr = G \int \int_{r'=0}^{R+H'} \rho(r', \Omega') \int \ell^{-1}(r, \psi, r') dr r'^2 dr' d\Omega'$$
(9)

To find the radial integral of the reciprocal distance  $\int \ell^{-1} dr$  on the right-hand side of Eq. (9), we first rearrange the expression  $r^2 + r'^2 - 2rrt\cos\psi = (r - rt\cos\psi)^2 + r'^2\sin^2\psi$ , and introduce two substitutions  $u = r - rt\cos\psi$  and du = dr. We then write



$$\int \ell^{-1} dr = \int \frac{1}{\sqrt{r^2 + r'^2 - 2rr'\cos\psi}} dr = \int \frac{1}{\sqrt{u^2 + r'^2\sin^2\psi}} du \tag{10}$$

Using the table of integrals, e.g., in (Gradshteyn and Ryzhik 2007), the solution of Eq. (10) is found to be.

$$\int \ell^{-1} dr = \ln \left| u + \sqrt{u^2 + r'^2 \sin^2 \psi} \right| + C \tag{11}$$

The substitution for  $u = r - r'os\psi$  in Eq. (11) yields.

$$\int \ell^{-1} dr = \ln \left| r - r' \cos \psi + \sqrt{r^2 + r'^2 - 2rr' \cos \psi} \right| + C = \ln \left| r - r' \cos \psi + \ell \left( r, \psi, r' \right) \right| + C$$

$$(12)$$

Inserting from Eq. (12) to Eq. (9), the radial integral of the Earth's gravitational potential *V* becomes

$$\int V dr = G \int \int_{0}^{R+H'} \rho(r', \Omega') \ln \left| r - r' \cos \psi + \ell(r, \psi, r') \right| r'^{2} dr' d\Omega'$$
 (13)

A primitive function of the radial integral of the Earth's gravitational potential  $\mathfrak{F}(r)$  is now defined in the following form:

$$\mathfrak{F}(r) = G \int \int_{0}^{R+H'} \rho(r', \Omega') \ln \left| r - r' \cos \psi + \ell(r, \psi, r') \right| r'^2 dr' d\Omega'$$
 (14)

It involves integration over the whole Earth's interior. It is worth noting that a closed-form (analytical) solution to the radial integral on the right-hand side of Eq. (14) does not exist.

Inserting the integration limits, the radial integral of the Earth's gravitational potential in Eq. (14) becomes

$$\begin{split} \mathfrak{F}(r_2) &- \mathfrak{F}(r_1) = \int\limits_{r_1}^{r_2} V dr = G \int\limits_0^{R+H'} \rho\left(r',\Omega'\right) \ln\left|r - r'\cos\psi + \ell\left(r,\psi,r'\right)\right| \Big|_{r_1}^{r_2} r'^2 dr' d\Omega' \\ &= G \int\limits_0^{R+H'} \int\limits_0^{r_1} \rho\left(r',\Omega'\right) \ln\left[\left|r_2 - r'\cos\psi + \ell\left(r_2,\psi,r'\right)\right| - \ln\left|r_1 - r'\cos\psi + \ell\left(r_1,\psi,r'\right)\right|\right] r'^2 dr' d\Omega' \\ &= G \int\limits_0^{R+H'} \int\limits_0^{r_1} \rho\left(r',\Omega'\right) \ln\left|\frac{r_2 - r'\cos\psi + \ell\left(r_2,\psi,r'\right)}{r_1 - r'\cos\psi + \ell\left(r_1,\psi,r'\right)}\right| r'^2 dr' d\Omega' \end{split}$$

$$(15)$$

## 2.3 Spherical Harmonic Series of the Radial Integral of the Earth's Gravitational Potential

The spherical harmonic representation of the Earth's gravitational potential V is given by (e.g., Heiskanen and Moritz 1967)

$$V(r,\Omega) = \frac{GM}{R} \sum_{n=0}^{\infty} \left(\frac{R}{r}\right)^{n+1} \sum_{m=-n}^{n} V_{n,m} Y_{n,m}(\Omega)$$
 (16)



where  $V_{n,m}$  are the (fully-normalized) numerical coefficients of the gravitational potential V of degree n and order m. The (fully-normalized) surface spherical functions  $Y_{n,m}$  in Eq. (16) are defined by

$$Y_{n,m}(\Omega) = P_{n,m}(\sin \varphi) \begin{cases} \cos m\lambda, & m \ge 0\\ \sin |m|\lambda, & m < 0, \end{cases}$$
(17)

where  $P_{n,m}$  are the (fully-normalized) associated Legendre functions.

The spherical harmonic representation of the radial integral of the Earth's gravitational potential in Eq. (16) is then given by

$$\int V dr = \frac{GM}{R} \sum_{n=0}^{\infty} \int \left(\frac{R}{r}\right)^{n+1} dr \sum_{m=-n}^{n} V_{n,m} Y_{n,m}(\Omega)$$

$$= \frac{GM}{R} \sum_{n=0}^{\infty} R^{n+1} \int \left(\frac{1}{r}\right)^{n+1} dr \sum_{m=-n}^{n} V_{n,m} Y_{n,m}(\Omega)$$

$$= \frac{GM}{R} \sum_{n=0}^{\infty} R^{n+1} \int r^{-n-1} dr \sum_{m=-n}^{n} V_{n,m} Y_{n,m}(\Omega)$$
(18)

The radial integral of  $r^{-n-1}$  on the right-hand side of Eq. (18) is found to be

$$\int r^{-n-1} dr = \begin{cases} \ln r + C & (n=0) \\ -\frac{1}{n} r^{-n} + C & (n>0) \end{cases}$$
 (19)

Substitution from Eq. (19) back to Eq. (18) yields

$$\int V dr = GM (\ln r + C) - GM \sum_{n=1}^{\infty} R^n \left( \frac{r^{-n}}{n} + C \right) \sum_{m=-n}^{n} V_{n,m} Y_{n,m}(\Omega)$$
 (20)

Setting C = 0, the indefinite radial integral of the Earth's gravitational potential in Eq. (20) becomes

$$\int V dr = GM \ln r - GM \sum_{n=1}^{\infty} \frac{1}{n} \left(\frac{R}{r}\right)^n \sum_{m=-n}^{n} V_{n,m} Y_{n,m}(\Omega)$$
 (21)

Inserting the upper and lower integration limits  $r_2$  and  $r_1$ , respectively, in Eq. (21), the radial integral of the Earth's gravitational potential in spherical harmonics becomes

$$\int_{r_{1}}^{2} V dr = GM \ln r \Big|_{r_{1}}^{r_{2}} - GM \sum_{n=1}^{\infty} \frac{R^{n}}{n} \Big|_{r_{1}}^{r_{2}} \sum_{m=-n}^{n} V_{n,m} Y_{n,m}(\Omega)$$

$$= GM \left( \ln r_{2} - \ln r_{1} \right) - GM \sum_{n=1}^{\infty} \frac{R^{n}}{n} \left[ r_{2}^{-n} - r_{1}^{-n} \right] \sum_{m=-n}^{n} V_{n,m} Y_{n,m}(\Omega)$$

$$= GM \ln \frac{r_{2}}{r_{1}} - GM \sum_{n=1}^{\infty} \frac{R^{n}}{n} \left[ \left( \frac{1}{r_{2}} \right)^{n} - \left( \frac{1}{r_{1}} \right)^{n} \right] \sum_{m=-n}^{n} V_{n,m} Y_{n,m}(\Omega)$$

$$= GM \ln \frac{r_{2}}{r_{1}} - GM \sum_{n=1}^{\infty} \frac{R^{n}}{n} \frac{r_{1}^{n} - r_{2}^{n}}{r_{2}^{n} r_{1}^{n}} \sum_{m=-n}^{n} V_{n,m} Y_{n,m}(\Omega)$$

$$= GM \ln \frac{r_{2}}{r_{1}} - GM \sum_{n=1}^{\infty} \frac{R^{n}}{n} \frac{r_{1}^{n} - r_{2}^{n}}{r_{2}^{n} r_{1}^{n}} \sum_{m=-n}^{n} V_{n,m} Y_{n,m}(\Omega)$$



As seen in Eq. (22), the radial integral of the gravitational potential consists of two terms. The first term defines the radial integral of potential generated by a radially symmetric mass density body. The first- and higher-degree spherical harmonics in the second term describe the respective contribution of anomalous mass density heterogeneities (with respect to a radially symmetric mass density distribution).

#### 2.4 Radial Integral of the Earth's Gravity Potential

The Earth's centrifugal potential  $\Phi$  is defined by

$$\Phi = \frac{1}{2}\overline{\omega}^2 r^2 \sin^2 \theta \tag{23}$$

where  $\overline{\omega}$  is the mean Earth's angular velocity, with the unit rad s<sup>-1</sup>. As seen in Eq. (23), the Earth's centrifugal potential  $\Phi$  is a function of the uniform Earth's rotational velocity  $\overline{\omega}$  and the perpendicular distance from the Earth's axis of rotation defined in terms of the geocentric radius r and the spherical co-latitude  $\theta$ .

From Eq. (23), the radial integral of the Earth's centrifugal potential is obtained in the following form:

$$\int \Phi dr = \frac{1}{2}\overline{\omega}^2 \sin^2 \theta \int r^2 dr = \frac{1}{6}\overline{\omega}^2 r^3 \sin^2 \theta \tag{24}$$

The radial integral of the geopotential W (i.e., the sum of the Earth's gravitational and centrifugal potentials V and  $\Phi$ , i.e.,  $W = V + \Phi$ ) is then given by

$$\int W dr = \int V dr + \int \Phi dr \tag{25}$$

Combining Eqs. (15) and (24), the radial integral of the geopotential is defined by:

$$\int_{r_{1}}^{r_{2}} W dr = G \int \int_{0}^{R+H'} \rho(r', \Omega') \ln \left| \frac{r_{2} - r' \cos \psi + \ell(r_{2}, \psi, r'r')}{r_{1} - r' \cos \psi + \ell(r_{1}, \psi, r'r')} \right| r'^{2} dr' d\Omega' + \frac{1}{6} \overline{\omega}^{2} (r_{2}^{3} - r_{1}^{3}) \sin^{2} \theta$$
(26)

The corresponding expression in spherical harmonics reads

$$\int_{r_1}^{r_2} W dr = GM \ln \frac{r_2}{r_1} - GM \sum_{n=1}^{\infty} \frac{R^n}{n} \frac{r_1^n - r_2^n}{r_2^n r_1^n} \sum_{m=-n}^n V_{n,m} Y_{n,m}(\Omega) + \frac{1}{6} \overline{\omega}^2 \left(r_2^3 - r_1^3\right) \sin^2 \theta$$
(27)

#### 2.5 Radial Integral of the Earth's Disturbing Gravity Potential

In physical geodesy, the disturbing gravity potential, gravity disturbances, and gravity anomalies are used in computations of the gravimetric geoid (e.g., Heiskanen and Moritz 1967; Bayoud and Sideris 2003). Note that in gravimetric geophysics, various types of gravity anomalies (such as the free-air, Bouguer or mantle gravity anomalies) are used to interpret the Earth's inner structure (e.g., McKenzie 1967; Watts and Talwani 1974; McKenzie and Fairhead 1997; Phillips and Lambeck 1980; Panet et al. 2014). These quantities are obtained from the Earth's gravity field parameters by subtracting respective parameters of



the normal gravity field (model gravity field generated by a rotating level biaxial ellipsoid). The disturbing potential T is defined as the difference between the Earth's gravity potential W and the normal gravity potential U, i.e., T = W - U. The gravity disturbance  $\delta g$  is defined as  $\delta g = g - \gamma$ , where g is the actual gravity and  $\gamma$  is the normal gravity, both stipulated at the same point (their magnitudes are measured and often approximated by radial vector components). The gravity anomaly  $\Delta g$  is defined in spherical approximation as  $\Delta g = \delta g - 2r^{-1}T$ . We note that the gravity anomaly is typically defined as the difference between the actual gravity g at the geoid and the normal gravity  $\gamma$  at the reference ellipsoid (e.g., Heiskanen and Moritz 1967), while a more rigorous definition was given by Vaníček et al. (2005).

The disturbing potential T in spherical harmonics reads (Heiskanen and Moritz 1967)

$$T(r,\Omega) = \frac{GM}{R} \sum_{n=0}^{\infty} \left(\frac{R}{r}\right)^{n+1} \sum_{m=-n}^{n} T_{n,m} Y_{n,m}(\Omega)$$
 (28)

where  $T_{n,m}$  are (fully-normalized) numerical coefficients of the disturbing potential T of degree n and order m obtained from the (fully-normalized) numerical coefficients  $V_{n,m}$  of the Earth's gravitational potential V (estimated from observed gravity data) after subtracting the respective numerical coefficients of the normal gravity field (defined analytically). Note that the centrifugal potential is absent in Eq. (28) as both the real and normal fields include the same centrifugal potential.

By analogy with Eq. (22), the radial integral of the disturbing potential T is defined in the following form:

$$\int_{r_1}^{r_2} T dr = GM \ln \frac{r_2}{r_1} - GM \sum_{n=1}^{\infty} \frac{R^n}{n} \frac{r_1^n - r_2^n}{r_2^n r_1^n} \sum_{m=-n}^n T_{n,m} Y_{n,m}(\Omega)$$
 (29)

The expressions in Eq. (28) and (29) include zero- and first-degree spherical harmonics. If we consider that the total mass of the Earth is equal to the mass of the reference ellipsoid, and the center of the Earth's masses coincides with the origin of the adopted coordinate system, then the summation begins from degree two, so that

$$\int_{r_1}^{r_2} T dr = -GM \sum_{n=2}^{\infty} \frac{R^n}{r_1^n} \frac{r_1^n - r_2^n}{r_2^n r_1^n} \sum_{m=-n}^n T_{n,m} Y_{n,m}(\Omega)$$
(30)

# 3 Functional Relations Between the Radially Integrated Disturbing Potential and Other Gravity Field Parameters

Let us assume that the gravity field above the geoid is harmonic, i.e., the disturbing potential satisfies the Laplace equation, i.e.,  $\nabla^2 T = 0$  for r > R. Mathematically, this is realized by subtracting the gravitational potentials of topographic and atmospheric masses from the geopotential. For gravity parameters satisfying the Laplace equation, we can use the Poisson, Hotine, and Stokes surface integrals and introduce respective solutions for their radial integrals that link the radial integral of the disturbing potential with values of the disturbing potential, the gravity disturbance, and the gravity anomaly at the geoid. The proof of analytical solutions of radial integrals of Poisson, extended Hotine, and extended Stokes kernels (presented below) is given in appendix.



Let us first define the radial integral of the disturbing potential as a function of the disturbing potential at the geoid. This functional relation can be found by radially integrating the Poisson integral that defines the disturbing potential above the geoid in terms of the surface spherical integral of disturbing potential values at the geoid, i.e.,

$$T(r,\Omega) = \frac{R}{4\pi} \int P(r,\psi,R) T(R,\Omega') d\Omega'$$
(31)

The isotropic spherical Poisson integral kernel function P in Eq. (31) reads

$$P(r, \psi, R) = \frac{r^2 - R^2}{\ell^3(r, \psi, R)}$$
(32)

where the Euclidean spatial distance is defined as  $\ell(r, \psi, R) = \sqrt{r^2 + R^2 - 2rR\cos\psi}$ .

From Eq. (31), the radial integral of the disturbing potential is defined by means of the radial integral of the Poisson kernel in the following form:

$$\int T(r)dr = \frac{R}{4\pi} \int \int P(r, \psi, R)dr T(R, \Omega') d\Omega'$$
(33)

The solution of the radial integral of the Poisson kernel  $\int P dr$  is found to be

$$\int P(r, \psi, \mathbf{R}) dr = \int \frac{r^2 - \mathbf{R}^2}{\ell^3(r, \psi, \mathbf{R})} dr = \tanh^{-1} \left[ \frac{r - \mathbf{R} \cos \psi}{\ell(r, \psi, \mathbf{R})} \right] - \frac{2r}{\ell(r, \psi, \mathbf{R})} + \mathbf{C}$$
(34)

We note that the solution for the radially integrated Poisson kernel can be described in terms of natural logarithm instead of inverse hyperbolic tangent in the first term on the right-hand side Eq. (34), so that

$$\int P(r, \psi, \mathbf{R}) dr = \ln[\ell(r, \psi, \mathbf{R}) + r - \mathbf{R} \cos \psi] - \frac{2r}{\ell(r, \psi, \mathbf{R})} + \mathbf{C}.$$

In a similar way, we can define the radially integrated disturbing potential as a function of gravity disturbances at the geoid by utilizing the Hotine integral.

The extended (generalized) Hotine integral is defined by

$$T(r,\Omega) = \frac{R}{4\pi} \int H(r,\psi,R) \, \delta g(R,\Omega') d\Omega'$$
 (35)

where the extended Hotine kernel function in Eq. (35) reads

$$H(r, \psi, \mathbf{R}) = \frac{2\mathbf{R}}{\ell(r, \psi, \mathbf{R})} - \ln \frac{\ell(r, \psi, \mathbf{R}) + \mathbf{R} - r\cos\psi}{r(1 - \cos\psi)}$$
(36)

By analogy with Eq. (33), the radial integral of the disturbing potential is written in the following form:

$$\int T(r)dr = \frac{R}{4\pi} \int \int H(r, \psi, R)dr \, \delta g(R, \Omega')d\Omega'$$
(37)

where  $\delta g$  denotes the gravity disturbance.

The radial integral of the Hotine kernel  $\int H dr$  is found to be



$$\int H(r, \psi, R) dr = \int \frac{2R}{\ell(r, \psi, R)} dr - \int \ln[\ell(r, \psi, R) + R - r\cos\psi] dr + \int \ln[r(1 - \cos\psi)] dr 
= 2R \ln[\ell(r, \psi, R) + r - R\cos\psi] - r \ln[\ell(r, \psi, R) + R - r\cos\psi] 
-R \ln[\ell(r, \psi, R) + r - R\cos\psi] + r + r \{\ln[r(1 - \cos\psi)] - 1\} + C 
= R \ln[\ell(r, \psi, R) + r - R\cos\psi] - r \ln[\ell(r, \psi, R) + R - r\cos\psi] + r + r \{\ln[r(1 - \cos\psi)] - 1\} + C 
(38)$$

By analogy with the solutions for the radially integrated Poisson kernel, the solution for the radially integrated Hotine kernel can be expressed in terms of natural logarithm as well as inverse hyperbolic tangent. We then write

$$\int H(r, \psi, R) dr = R \tanh^{-1} \left[ \frac{r - R \cos \psi}{\ell(r, \psi, R)} \right] - r \tanh^{-1} \left[ \frac{r - R \cos \psi}{\ell(r, \psi, R)} \right] + r + r \left\{ \ln \left[ r(1 - \cos \psi) \right] - 1 \right\} + C \ln \left[ r(1 - \cos \psi) \right] - C \ln \left[ r(1 - \cos \psi) \right$$

As seen in Eq. (37), the radial integral of the disturbing potential  $\int T dr$  can be computed from the gravity disturbances  $\delta g$  at the geoid.

The derivation of a functional relation between the radial integral of the disturbing potential  $\int T dr$  and the gravity anomalies  $\Delta g$  at the geoid involves the Stokes integral formula.

The extended (generalized) Stokes integral is defined by

$$T(r,\Omega) = \frac{1}{4\pi} \int S(r,\psi,R) \, \Delta g(R,\Omega') d\Omega' \tag{39}$$

where  $\Delta g$  is the gravity anomaly.

The extended Stokes kernel function in Eq. (39) is given by

$$S(r, \psi, \mathbf{R}) = \frac{2\mathbf{R}}{\ell(r, \psi, \mathbf{R})} + \frac{\mathbf{R}}{r} - 3\frac{\mathbf{R}}{r^2}\ell(r, \psi, \mathbf{R}) - \left(\frac{\mathbf{R}}{r}\right)^2 \cos\psi \left\{5 + 3\ln\left[\frac{\ell(r, \psi, \mathbf{R}) + r - \mathbf{R}\cos\psi}{2r}\right]\right\}$$
(40)

According to Eq. (39), the radial integral of the disturbing potential  $\int T dr$  can be obtained from the gravity anomalies  $\Delta g$  at the geoid. We then write

$$\int T(r)dr = \frac{R}{4\pi} \int \int S(r, \psi, R)dr \, \Delta g(R, \Omega')d\Omega'$$
(41)

The radial integral of the Stokes kernel function is found to be

$$f S(r, \psi, R) dr = 2R \int \frac{1}{\ell(r, \psi, R)} dr + R \int r^{-1} dr - 3R \int \frac{\ell(r, \psi, R)}{r^2} dr - 5R^2 \cos \psi \int r^{-2} dr$$

$$-3R^2 \cos \psi \int r^{-2} \ln \left[ \frac{\ell(r, \psi, R) + r - R \cos \psi}{2r} \right] dr = 2R \ln \left[ \ell(r, \psi, R) + r - R \cos \psi \right]$$

$$+R \ln (r) - 3R \left\{ -\frac{\ell(r, \psi, R)}{r} + \tanh^{-1} \left[ \frac{r - R \cos \psi}{\ell(r, \psi, R)} \right] + \cos \psi \tanh^{-1} \left[ \frac{R - r \cos \psi}{\ell(r, \psi, R)} \right] \right\}$$

$$+5 \cos \psi \frac{R^2}{r} - 3R^2 \cos \psi \left\{ \frac{1}{r} - \frac{1}{r} \ln \left[ \frac{\ell(r, \psi, R) + r - R \cos \psi}{2r} \right] - \frac{1}{R} \tanh^{-1} \left[ \frac{R - r \cos \psi}{\ell(r, \psi, R)} \right] \right\} + C$$

$$= 2R \ln \left[ \ell(r, \psi, R) + r - R \cos \psi \right] + R \ln (r) + 3R \left\{ \frac{\ell(r, \psi, R)}{r} - \tanh^{-1} \left[ \frac{r - R \cos \psi}{\ell(r, \psi, R)} \right] \right\}$$

$$+5 \cos \psi \frac{R^2}{r} - 3R^2 \cos \psi \left\{ \frac{1}{r} - \frac{1}{r} \ln \left[ \frac{\ell(r, \psi, R) + r - R \cos \psi}{2r} \right] \right\} + C$$

$$(42)$$



In addition to surface integrals for computing the radial integral of the disturbing potential from values of the disturbing potential, the gravity disturbance, and the gravity anomaly at the geoid, we introduce the relation between radial integrals of the disturbing potential and the gravity disturbance  $\int T dr$  and  $\int \delta g dr$ , respectively.

We first consider only the zero-degree terms T = GM/r and  $\delta g = GM/r^2$  of disturbing potential and gravity disturbance, respectively. We then write

$$\mathfrak{F}(r_2) - \mathfrak{F}(r_1) = \int_{r_1}^{r_2} T(r) \, \mathrm{d}r \tag{43}$$

and

$$T(r_1) - T(r_2) = -\int_{r_1}^{r_2} \frac{\partial T(r)}{\partial r} dr = \int_{r_1}^{r_2} \delta g(r) dr$$
(44)

Substituting for T = GM/r and  $\delta g = GM/r^2$  in Eqs. (43) and (44), we arrive at

$$\int_{r_1}^{r_2} T(r) dr = GM \ln \frac{r_2}{r_1}$$
 (45)

$$\int_{r_1}^{r_2} \delta g(r) dr = T(r_1) - T(r_2) = \frac{GM}{r_1} - \frac{GM}{r_2} = GM \frac{r_2 - r_1}{r_1 r_2}$$
(46)

We reorganize Eq. (46) as follows

$$\frac{r_1 r_2}{r_2 - r_1} \int_{r_1}^{r_2} \delta g(r) dr = GM \tag{47}$$

Combining Eqs. (45) and (47), we arrive at

$$\int_{r_1}^{r_2} T(r)dr = \ln \frac{r_2}{r_1} \frac{r_1 r_2}{r_2 - r_1} \int_{r_1}^{r_2} \delta g dr$$
 (48)

For  $r_2 - r_1 \ll R$  we have  $\ln r_2/r_1 \cong (r_2 - r_1)/r_1$ . The expression in Eq. (48) then becomes and

$$\int_{r_{1}}^{r_{2}} T(r)dr \cong \frac{r_{2} - r_{1}}{r_{1}} \frac{r_{1}r_{2}}{r_{2} - r_{1}} \int_{r_{1}}^{r_{2}} \delta g(r)dr$$

$$\int_{r_1}^{r_2} T(r)dr \cong r_2 \int_{r_1}^{r_2} \delta g(r)dr \tag{49}$$

For the first- and higher-degree terms of T and  $\delta g$ , i.e.,

$$T(r,\Omega) = \frac{GM}{R} \sum_{n=1}^{\infty} \left(\frac{R}{r}\right)^{n+1} \sum_{m=-n}^{n} T_{n,m} Y_{n,m}(\Omega)$$
 (50)

$$\delta g(r,\Omega) = \frac{GM}{R^2} \sum_{n=1}^{\infty} \sum_{m=-n}^{n} \left(\frac{R}{r}\right)^{n+2} (n+1) T_{n,m} Y_{n,m}(\Omega)$$
 (51)



the respective radial integrals  $\int T dr$  and  $\int \delta g dr$  are derived as follows:

We first write the radial integral of the disturbing potential  $\int T dr$  for  $n \ge 1$  in the following form

$$\int_{r_1}^{r_2} T dr = \frac{GM}{R} \sum_{n=1}^{\infty} R^{n+1} \int_{r_1}^{r_2} r^{-n-1} dr \sum_{m=-n}^{n} T_{n,m} Y_{n,m}(\Omega)$$
 (52)

Inserting for  $\int r^{-n-1} dr = -\frac{1}{n} r^{-n} + C$  in Eq. (52), we get

$$\int_{r_{1}}^{r_{2}} T(r)dr = -\frac{GM}{R} \sum_{n=1}^{\infty} \frac{R^{n+1}}{n} r^{-n} \Big|_{r_{1}}^{r_{2}} \sum_{m=-n}^{n} T_{n,m} Y_{n,m}(\Omega)$$

$$= -\frac{GM}{R} \sum_{n=1}^{\infty} \frac{R^{n+1}}{n} \left( \frac{1}{r_{2}^{n}} - \frac{1}{r_{1}^{n}} \right) \sum_{m=-n}^{n} T_{n,m} Y_{n,m}(\Omega)$$

$$= -GM \sum_{n=1}^{\infty} \frac{R^{n}}{n} \frac{r_{1}^{n} - r_{2}^{n}}{r_{2}^{n} r_{1}^{n}} \sum_{m=-n}^{n} T_{n,m} Y_{n,m}(\Omega)$$

$$= GM \sum_{n=1}^{\infty} \frac{R^{n}}{n} \frac{r_{2}^{n} - r_{1}^{n}}{r_{2}^{n} r_{1}^{n}} \sum_{m=-n}^{n} T_{n,m} Y_{n,m}(\Omega)$$
(53)

The radial integral of the gravity disturance  $\int \delta g dr$  for  $n \ge 1$  is defined by

$$\int_{r_1}^{r_2} \delta g(r) dr = \frac{GM}{R^2} \sum_{n=1}^{\infty} R^{n+2} \int_{r_1}^{r_2} r^{-n-2} dr (n+1) \sum_{m=-n}^{n} T_{n,m} Y_{n,m}(\Omega)$$
 (54)

For  $\int r^{-n-2} dr = -\frac{1}{n+1} r^{-n-1} + C$ , we have

$$\int_{r_{1}}^{r_{2}} \delta g(r) dr = -\frac{GM}{R^{2}} \sum_{n=1}^{\infty} R^{n+2} r^{-n-1} \Big|_{r_{1}}^{r_{2}} \frac{n+1}{n+1} \sum_{m=-n}^{n} T_{n,m} Y_{n,m}(\Omega)$$

$$= -\frac{GM}{R^{2}} \sum_{n=1}^{\infty} R^{n+2} \left( \frac{1}{r_{2}^{n+1}} - \frac{1}{r_{1}^{n+1}} \right) \sum_{m=-n}^{n} T_{n,m} Y_{n,m}(\Omega)$$

$$= \frac{GM}{R} \sum_{n=1}^{\infty} R^{n} \frac{r_{2}^{n+1} - r_{1}^{n+1}}{r_{2}^{n+1} r_{1}^{n+1}} \sum_{m=-n}^{n} T_{n,m} Y_{n,m}(\Omega)$$
(55)

Combing Eqs. (53) and (55), we arrive at

$$\frac{\int_{r_1}^{r_2} T(r)dr}{R \int_{r_1}^{r_2} \delta g(r)dr} = \frac{\sum_{n=1}^{\infty} \frac{R^n}{n} \frac{\frac{r_2^n - r_1^n}{r_2^n r_1^n}}{\sum_{m=-n}^{\infty} T_{n,m} Y_{n,m}(\Omega)}}{\sum_{n=1}^{\infty} R^n \frac{\frac{r_2^{n+1} - r_1^{n+1}}{r_2^{n+1} - r_1^{n+1}}}{\sum_{m=-n}^{n} T_{n,m} Y_{n,m}(\Omega)}}$$
(56)

## 4 Numerical Examples

Regional and global maps of the geoid (or less commonly used disturbing potential), the gravity anomalies/disturbances, and the gravity gradient have extensively been used in gravimetric interpretations of the Earth's inner structure. To briefly review the most



pronounced spatial features in these gravity field parameters, we computed and plotted global maps of the geoid N, the gravity disturbance  $\delta g$ , and the disturbing gravity gradient  $\Gamma$ . The spatial patterns in the geoidal geometry and the disturbing potential are obviously the same because the geoid height is defined as the disturbing potential T at the geoid divided by the normal gravity  $\gamma_0$  at the reference ellipsoid, i.e.,  $N = T/\gamma_0$ . We also note that spatial patterns in maps of gravity anomalies and gravity disturbances are very similar (cf. Vajda et al. 2007). The computation was realized globally on the 1 arc-deg equiangular coordinate grid using the EIGEN-6C4 (Förste et al. 2014) coefficients (for spherical harmonic degrees: n=2,3,...,2160) according to the following equations:

$$N = \frac{T(R, \Omega)}{\gamma_0} = \frac{1}{\gamma_0} \frac{GM}{R} \sum_{n=2}^{2160} \sum_{m=-n}^{n} T_{n,m}^T Y_{n,m}(\Omega)$$
 (57)

$$\delta g = \delta g(\mathbf{R}, \Omega) \cong -\frac{\partial T}{\partial r} = \frac{\mathbf{GM}}{R^2} \sum_{n=2}^{2160} (n+1) \sum_{m=-n}^{n} \mathbf{T}_{n,m}^T Y_{n,m}(\Omega)$$
 (58)

$$\Gamma \cong \frac{\partial^2 T}{\partial r^2} = \frac{GM}{R^2} \sum_{n=2}^{2160} (n+1)(n+2) \sum_{m=-n}^{n} T_{n,m}^T Y_{n,m}(\Omega)$$
 (59)

where  $\gamma_0$  is the normal gravity at the reference ellipoid GRS80 (Moritz 2000).

The global maps of geoid heights, gravity disturbances, and disturbing gravity gradients are shown in Fig. 1. As seen in Fig. 1a, the global geoid heights are roughly within ± 100 m. It is commonly understood that the long-wavelength geoidal geometry reflects a global mantle convection pattern with the most pronounced features of the Indian Ocean Geoid Low and the West Pacific and North Atlantic Geoid Highs (e.g., Hager et al. 1985; Hager and Richards 1989; Steinberger 2000). The additional geoid lows are in North America and Southwest Pacific, and the geoid high in Southwest Indian Ocean. Geoid undulations attributed to the topographic and ocean-floor relief as well as the lithospheric density structure are much less pronounced. Maximum geoid modifications by the topographic mass surplus of the Himalayas and Tibetan Plateau are up to ~30 m. The geoid modifications by elevated topography are also clearly recognized across central Andes. The marine geoid modifications by the ocean floor relief are most notable along oceanic subductions and volcanic arcs.

The spatial pattern of gravity disturbances, see Fig. 1b, is characterized by relatively small gravity anomaly fluctuations mostly within  $\pm$  100 mGal ( $\pm$  10<sup>-3</sup> m s<sup>-2</sup>). A long-wavelength mantle signature is still partially manifested even in the presence of much more pronounced lithospheric signature in the gravity map. Nevertheless, since most of major topographic features and large lithospheric density structures are in an isostatic equilibrium, the largest gravity variations (up to  $\pm$  5 × 10<sup>-3</sup> m s<sup>-2</sup>) mark mainly uncompensated lithospheric structures along active convergent tectonic margins (including mostly orogenic formations and oceanic subductions).

The disturbing gravity gradient globally varies within  $\pm 1.5 \times 10^{-7}$  s<sup>-2</sup>, with some of the largest variations detected along active convergent tectonic margins, see Fig. 1c. Nevertheless, this spatial pattern in the gravity gradient cannot primarily be attributed to tectonic features. Rather, it largely reflects a complex terrain and ocean floor relief, while partially also horizontal gravity changes across margins of significantly different geological units. A long-wavelength mantle signature in the gravity gradient map is completely absent.

The geoid, gravity, and gravity gradient maps in Fig. 1 clearly demonstrate that the application of the gradient operator to the (disturbing) gravity potential enhances a



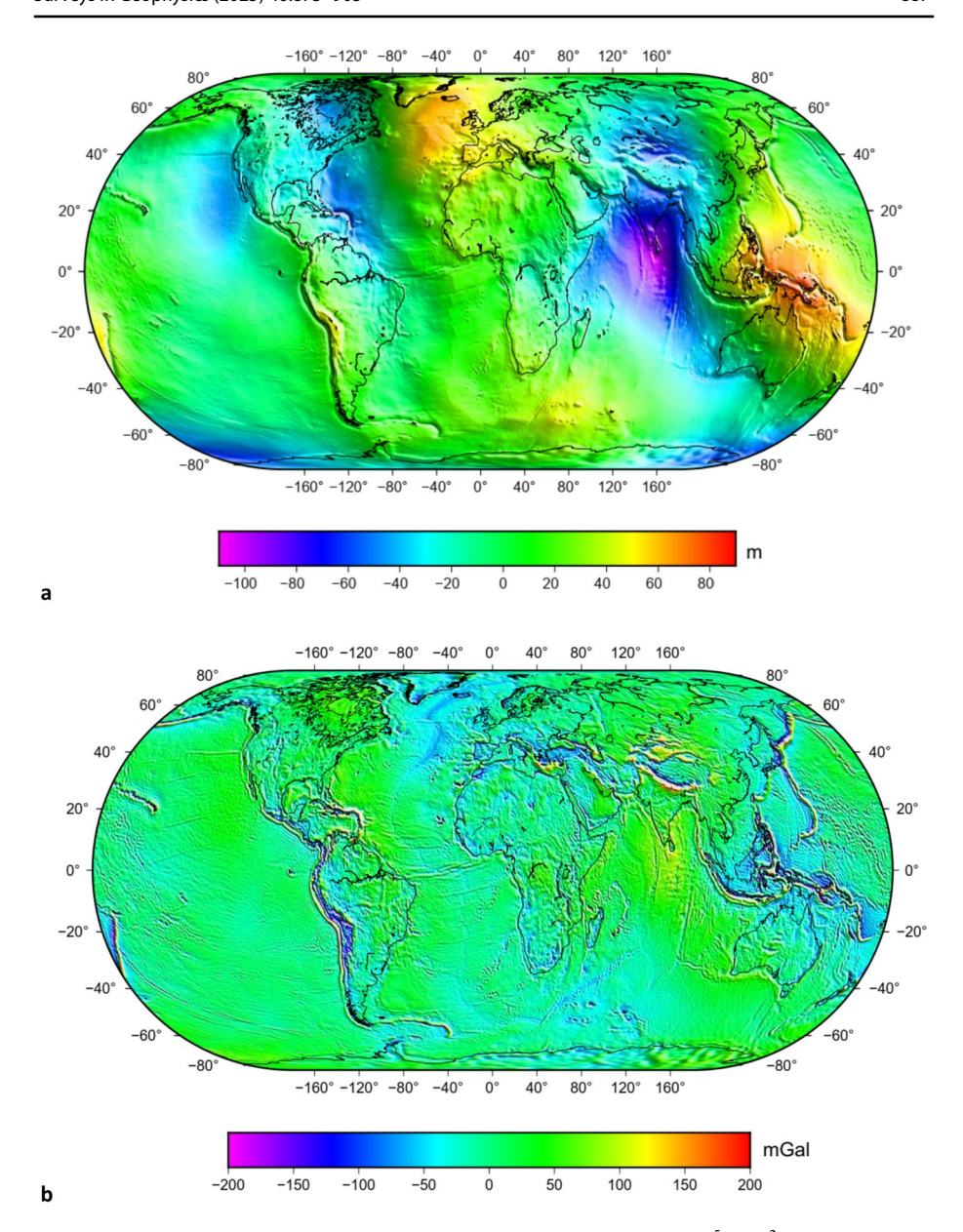


Fig. 1 Global maps of: a geoid heights (m), b gravity disturbances (mGal =  $10^{-5}$  m s<sup>-2</sup>), and c disturbing gravity gradients (eotvos =  $10^{-9}$  s<sup>-2</sup>) computed on the 1 arc-deg equiangular grid using the EIGEN-6C4 coefficients (n = 2, 3, ..., 2160)

lithospheric signature in the gravity map, and a more detailed pattern of the topographic and ocean floor relief in the gravity gradient map, while the geoidal geometry is dominated by a long-wavelength mantle signature. Consequently, it is expected that the application of radial integral operator will have opposite effect, thus smoothing the geoidal geometry (and equivalently the disturbing potential). To inspect this assumption, we computed and plotted



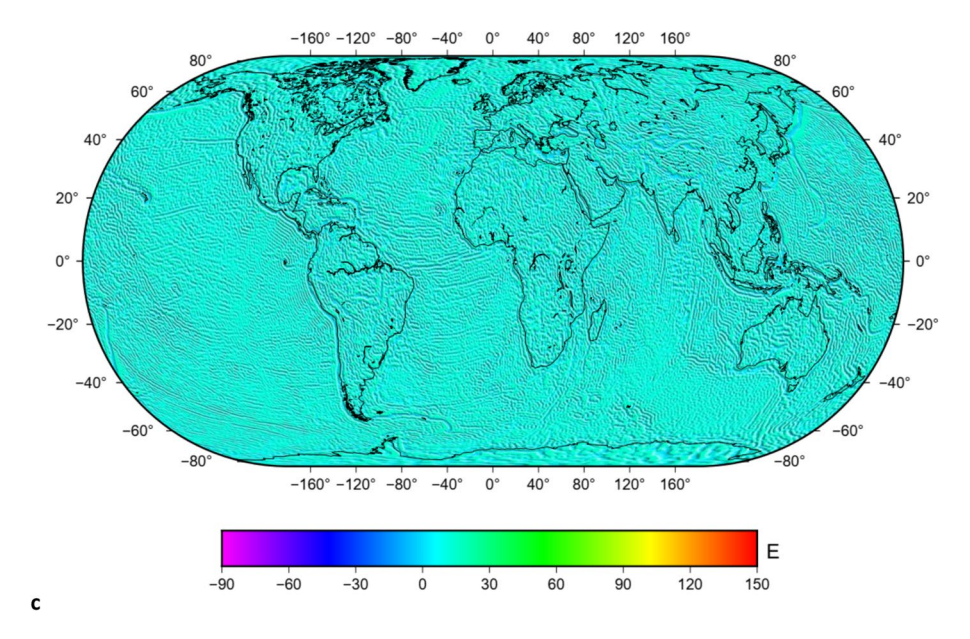


Fig. 1 (continued)

the indefinite radial integral of the disturbing potential, i.e.,  $\Im(r)$  for r = R. The computation was again realized globally on the 1 arc-deg equiangular grid using the EIGEN-6C4 coefficients (n = 2, 3, ..., 2160) according to the following formula:

$$\mathfrak{F}(R,\Omega) = GM \sum_{n=0}^{2160} \frac{1}{n} \sum_{m=-n}^{n} T_{n,m} Y_{n,m}(\Omega)$$
 (60)

As seen in Eq. (60), the spherical harmonics  $T_{n,m}$  of the disturbing potential are in this case scaled by the factor 1/n. Consequently, this scaling factor lessens the contribution of higher-degree spherical harmonics so that their combined contribution in the indefinite radial integral of the disturbing potential become significantly smaller than in the geoidal geometry, see Eq. (57). This is evident in Fig. 2, where we plotted the result of Eq. (60), computed again on the 1 arc-deg equiangular grid using the EIGEN-6C4 coefficients (n=2, 3, ..., 2160).

A deep mantle structure, dominated by two large antipodal low shear-velocity provinces at the base of the mantle (e.g., Steinberger 2000), is to some extent manifested in the geoidal geometry, see Fig. 1a, by two large positive anomalies that are coupled by large negative anomalies attributed to mantle downwelling in mantle convection. The same long-wavelength pattern can also be recognized in the radially integrated disturbing potential, see Fig. 2, while the lithospheric signature is in this result much less pronounced than in the geoidal geometry. The main reason is that the lithospheric signature remains apparent in the long-wavelength geoidal geometry computed from low-degree spherical harmonics of the disturbing potential. Similarly, the spectral filtering could not completely remove the lithospheric signature from the geoidal geometry. This is evident from Figs. 3 and 4, where we plotted the long-wavelength geoid models (for the maximum degree of spherical harmonics between degrees 5 and 25, with a 5-degree step)



and the spectrally filtered geoid models, respectively. We note that the Gauss filter was applied for radii of 4000, 2000, 1300, 1000 and 800 km that closely correspond to maximum degrees of spherical harmonics used in the spectral decomposition in terms of a half-wavelength. We see, for instance, that the gravitational signature of Andes is absent only in the geoid model computed to degree 5 of spherical harmonics, see Fig. 3a, while is present in all filtered solutions, see Fig. 4a–e. In contrast, the gravitational signature of these large orogenic formations is not clearly manifested in the radially integrated disturbing potential (Fig. 2). Consequently, the application of radial integral operator in combination with the gravimetric forward modeling of lithospheric density structure (cf. Tenzer et al. 2009; 2012; 2015; Tenzer and Chen 2019) using improved seismic tomography, mineralogy, density and topography/bathymetry models can be beneficial for interpreting lateral density variations within mantle.

We further investigated the power spectra of the radially integrated disturbing potential, the disturbing potential, the gravity disturbance, and the disturbing gravity gradient. For this purpose, we compared the degree variances and the cumulative degree variances of gravity field parameters involved. The power spectrum analysis is plotted in Fig. 5.

For the radial integral of the disturbing potential, the computation of degree variances (for  $\bar{n} = 2160$ ) was carried out according to Parseval's generalized theorem (Gelderen van and Koop, 1997)

$$\sigma_n^2 \left( \int T dr \right) = \frac{1}{n^2} \sum_{m=-n}^n \left( T_{n,m} \right)^2$$
 (61)

where  $T_{n,m}$  are the coefficients of the disturbing potential. The corresponding cumulative degree variances were calculated from

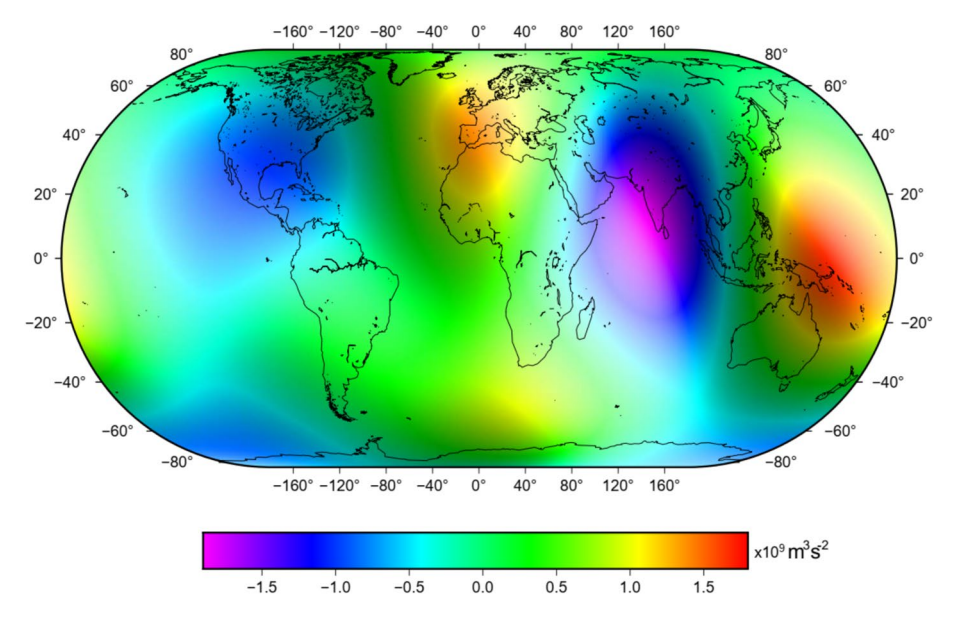


Fig. 2 Global map of the indefinite radial integral of the disturbing potential ( $m^3$  s<sup>-2</sup>) computed on the 1 arc-deg equiangular grid using the EIGEN-6C4 coefficients (n = 2, 3, ..., 2160)



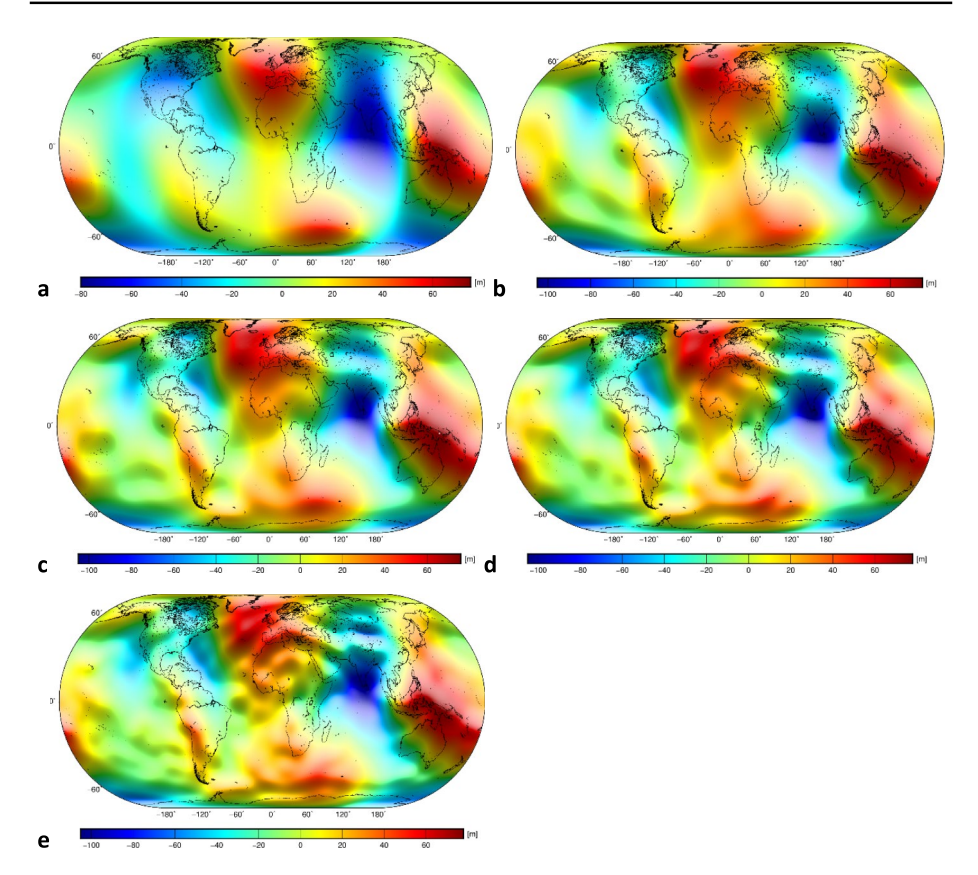


Fig. 3 Global maps of long-wavelength geoid models computed on the 1 arc-deg equiangular grid using the EIGEN-6C4 coefficients with a spectral resolution complete to a maximum degree of: **a** 5, **b** 10, **c** 15, **d** 20, and **e** 25

$$\Theta_N(\int T dr) = \sum_{n=2}^{\bar{n}} \sigma_n^2(\int T dr) = \sum_{n=2}^{\bar{n}} \frac{1}{n^2} \sum_{m=-n}^n (T_{n,m})^2$$
 (62)

For the disturbing potential, the gravity disturbance, and the disturbing gravity gradient, the respective expressions for computation of the degree variances are  $\sigma_n^2(T) = \sum_{m=-n}^n \left(T_{n,m}\right)^2$ ,  $\sigma_n^2(\delta g) = (n+1)^2 \sum_{m=-n}^n \left(T_{n,m}\right)^2$ , and  $\sigma_n^2(\Gamma) = (n+1)^2 (n+2)^2 \sum_{m=-n}^n \left(T_{n,m}\right)^2$ .

As seen in Fig. 5a, the disturbing gravity gradient has the lagest signal at the whole spectrum (up to n=2160) among the investigated gravity field parameters, with typically increasing energy at long-wavelengths (up to degree -120) and a slightly weakening energy beyond degree -300. The power spectra of the disturbing potential, gravity disturbance and the radially integrated disturbing potential are, on the other hand, characterized by a weakening energy at the whole spectrum, most remarkably in the spectrum of the radially integrated disturbing potential, while much less in the potential spectrum (i.e., the geoidal geometry). In the gravity spectrum, the signal attenuates much more moderately (after degree -20), while the gravity gradient spectrum (beyond degree -120) has very stable energy. This finding confirmed that



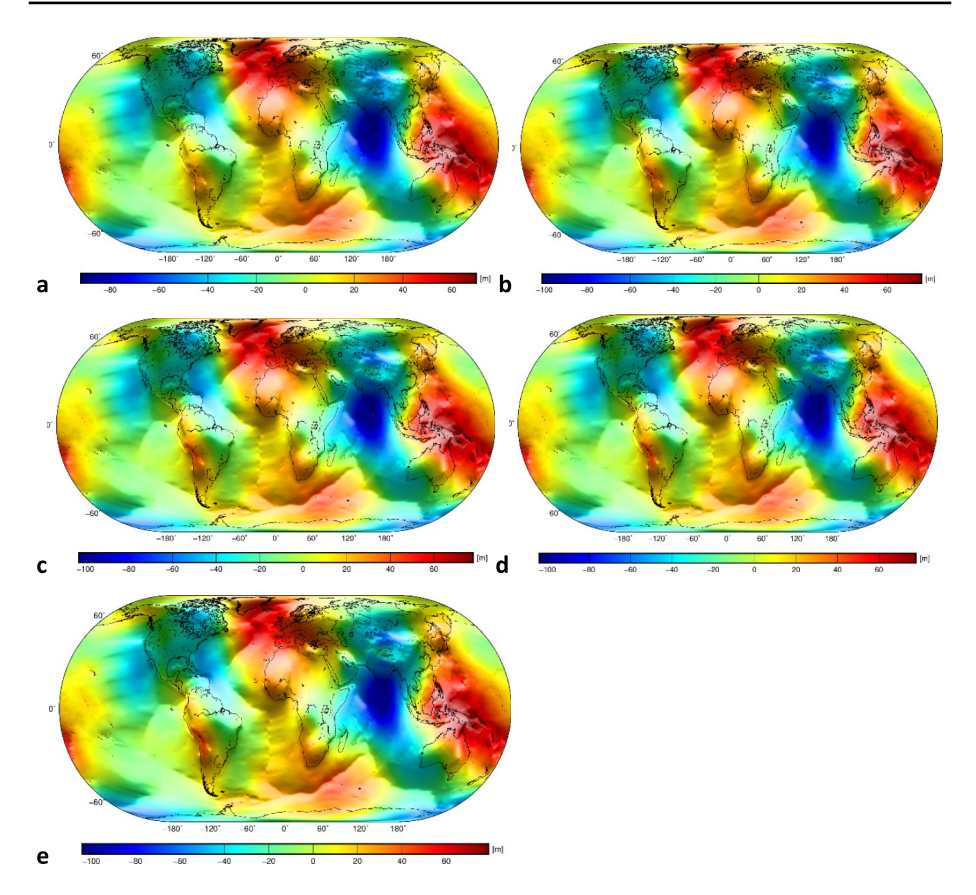


Fig. 4 Global maps of long-wavelength geoid models obtained after applying the Gaussian filter with the radius of: **a** 4000 km, **b** 2000 km, **c** 1300 km, **d** 1000 km, and **e** 800 km. The original geoid model was computed on the 1 arc-deg equiangular grid using the EIGEN-6C4 coefficients (n=2, 3, ..., 2160)

the application of gradient operator gradually enhances the gravitational signature of more detailed geological, tectonic, and topographic features with the increasing degree of spherical harmonics. Spectral characteristics of the gravity field parameters, see Fig. 5a, are directly manifested in their respective cumulative degree variances, see Fig. 5b. Most of the energy in the radially integrated disturbing potential and the disturbing potential is accumulated at very low degrees of spherical harmonics (up to degree -10). The same finding applies to the gravity disturbances, but in this case, we see an additional moderate energy increase (up to degree -200). In contrast, the energy of the gravity gradient signal increases at the entire spectrum investigated up to degree 2160.

Finally, we compared the difference between the integral mean of the disturbing potential and the disturbing potential at the geoid. The differences were computed as follows

$$\frac{1}{H} \int_{R}^{R+H} T dr - T_g = \frac{1}{H} GM \sum_{n=2}^{2160} \frac{1}{n} \left[ 1 - \left( \frac{R}{R+H} \right)^n \right] \sum_{m=-n}^{n} T_{n,m} Y_{n,m}(\Omega) - \frac{GM}{R} \sum_{n=2}^{2160} \sum_{m=-n}^{n} T_{n,m} Y_{n,m}(\Omega)$$
(63)



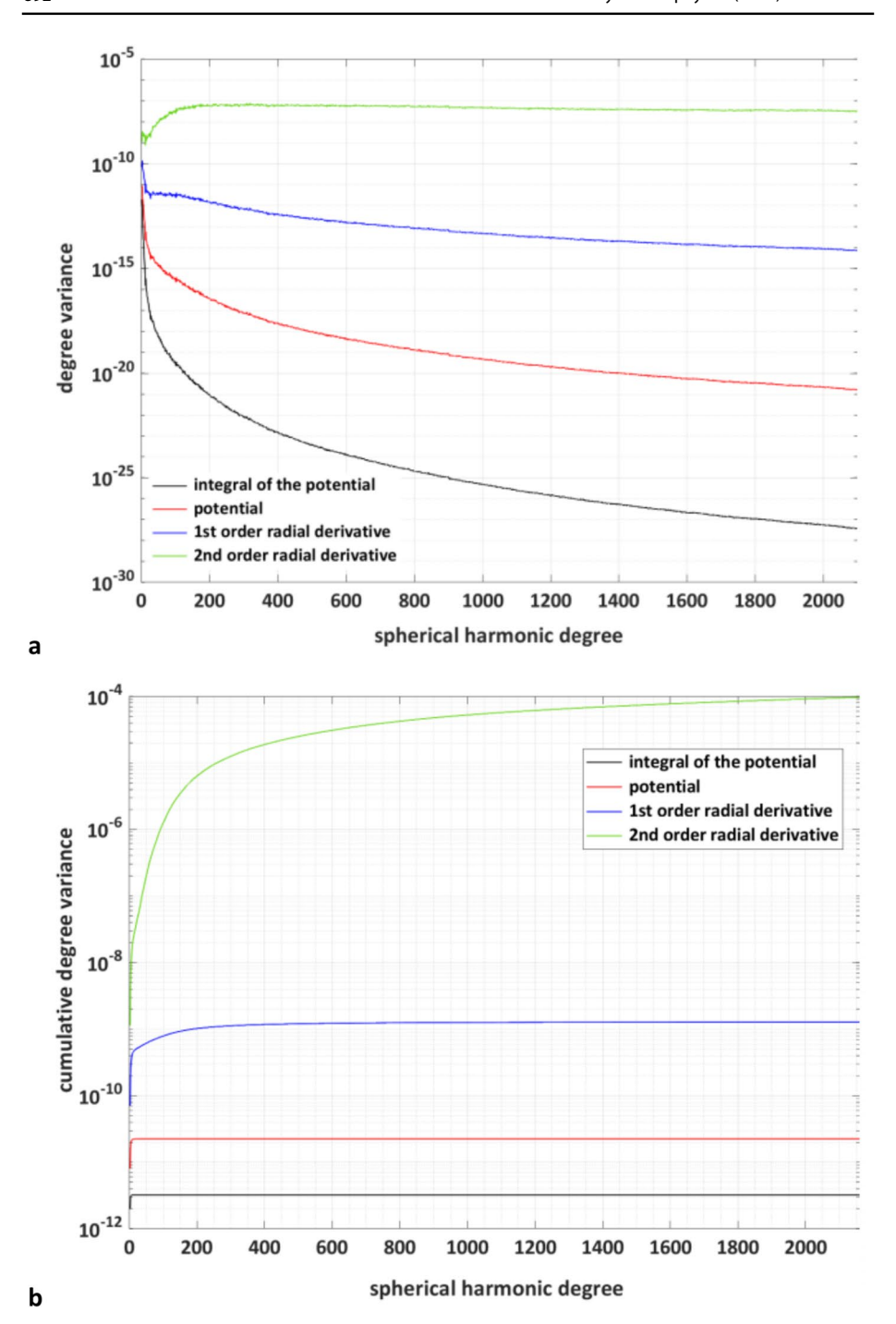


Fig. 5 Power spectrum of the gravity field parameters: a degree variances and b cumulative degree variances (for spherical harmonic degrees coefficients n=2, 3, ..., 2160). Log scale is used for the vertical axis



where the interval of radial integration was taken from the geoid up to the height  $H=1\times 10^4$  m, i.e.,  $r\in \langle R,R+H\rangle$ . The result is shown on Fig. 6. We note that the integral mean of the disturbing potential was computed instead of the radial integral of the disturbing potential to have the same units for both parameters, i.e., the radial integral of the disturbing potential was scaled by the factor  $H^{-1}$  to get values of  $\frac{1}{H}\int_{R}^{R+H}T\mathrm{d}r$  in m<sup>2</sup> s<sup>-2</sup> as for the disturbing potential T.

As seen in Fig. 6, differences between the integral mean of the disturbing potential and the disturbing potential do not exhibit a long-wavelength mantle signature. Instead, more detailed patterns of the largest vertical changes of disturbing potential are revealed that closely resemble the gravity map in Fig. 1b. In other words, the mean values of the disturbing potential at the radial interval  $r \in \langle R, R + H \rangle$  for  $H = 1 \times 10^4$  m, only slightly differ from values of the disturbing potential at the geoid.

## 5 Summary and Concluding Remarks

We have introduced the concept of the radial integral of the geopotential and investigated its possible applications. In the theoretical part, we defined this functional in spatial and spectral domains, and then derived its relations with other parameters of the Earth's gravity field. According to our results, the radially integrated gravitational potential generated by a radially symmetric mass density body (or point mass), i.e., the zero-degree spherical harmonic representation of the gravitational potential, is defined as the product of the geocentric gravitational constant GM and the natural logarithm of the geocentric distancer, i.e.,  $\mathfrak{F} = \int V dr = GM \ln r$ . The radially integrated gravitational potential has thus the same unit (m³ s<sup>-2</sup>) asGM. When

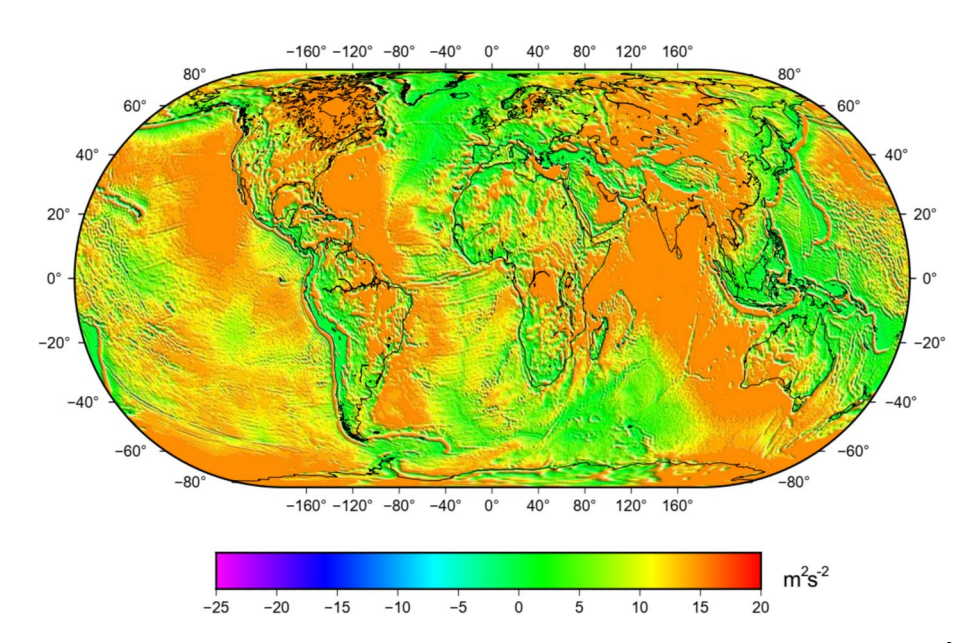


**Fig. 6** Differences between the integral mean of the disturbing potential and the disturbing potential ( $m^2$  s<sup>-2</sup>) at the geoid computed globally on the 1 arc-deg equiangular grid using the EIGEN-6C4 coefficients (n=2, 3, ..., 2160)



taking into consideration the respective expression for the gravitational potential (of a radially symmetric mass density body), i.e., V = GM/r, we see that the gravitational potential is inversely proportional to the geocentric distance, so that it monotonically decreases with the distance (when adopting geodetic conventions for the definition of potential), whereas its indefinite radial integral function, i.e., the primitive function of radially integrated gravitational potential, monotonically increases. In the spectral expression for the radially integrated gravitational potential generated by a heterogonous mass density body, the first- and higher-degree spherical harmonics of the gravitational potential ( $n \ge 1$ ) are scaled by the factor 1/n, thus reducing the contribution of higher-degree spherical harmonic terms.

In numerical examples, we demonstrated that the radial integration of (disturbing) potential smooths the solution, see Fig. 2. This implies that the application of gradient operator to the indefinite radial integral of the disturbing potential (that represents the reverse mathematical operation) must exhibit a more detailed pattern in the disturbing potential, or equivalently in the geoidal geometry, see Fig. 1a. This is obviously consistent with the fact that the gradient operator "roughens" spatially the solution. The application of gradient operator to the disturbing potential superimposes the lithospheric signature over a mantle signal in the gravity disturbance map, see Fig. 1b. Consequently, the application of gradient operator to the gravity disturbance exhibits the signature of topographic and ocean floor relief while completely removes a mantle signature in the gravity gradient map, see Fig. 1c.

#### 5.1 Proof of the Radially Integrated Poisson Kernel

Since the direct derivation of the analytical solution for the radially integrated Poisson kernel comprises extensive algebraic operations, we provide the proof of the final solution in the form of the radial derivative of indefinite radial integral of the Poisson kernel that obviously yields the Poisson kernel.

**Proposition 1:** According to Eqs. (34), the closed analytical solutions of the radial integral of the Poisson kernel read.

$$\int P(r, \psi, R) dr = \int \frac{r^2 - R^2}{\ell^3(r, \psi, R)} dr = \tanh^{-1} \left[ \frac{r - R\cos\psi}{\ell(r, \psi, R)} \right] - \frac{2r}{\ell(r, \psi, R)} + C$$

and

$$\int P(r, \psi, R) dr = \ln[\ell(r, \psi, R) + r - R\cos\psi] - \frac{2r}{\ell(r, \psi, R)} + C$$

Based on Lemma 1, it could readily be shown that both solutions for the radial integral of the Poisson kennel are equivalent. As seen, the first term can be written either in the form of inverse hyperbolic tangent or natural logarithm functions.

**Proof:** To provide the proof for the first term in the first solution, see Proposition 1, we define the following relation.

$$\frac{\partial}{\partial x} \tanh^{-1} u = \frac{1}{1 - u^2} \frac{\partial u}{\partial x} \tag{A.6}$$

where the substitution x is given in Eq. (A.4).



The radial derivative of the solution in Eq. (A.6) is given by

$$\frac{\partial}{\partial r} \tanh^{-1} \left[ \frac{r - R \cos \psi}{\ell(r, \psi, R)} \right] = \frac{\ell^2(r, \psi, R)}{R^2 \left( 1 - \cos^2 \psi \right)} \frac{R^2 \left( 1 - \cos^2 \psi \right)}{\ell^3(r, \psi, R)} = \frac{1}{\ell(r, \psi, R)} \tag{A.7}$$

The radial derivative of the second term (in the first solution of the radially integrated Poisson kernel) yields

$$\frac{\partial}{\partial r} \frac{2r}{\ell(r, \psi, R)} = \frac{-2R + 2R \, r \cos \psi}{\ell^3(r, \psi, R)} \tag{A.8}$$

According to Lemma 1, we get

$$\frac{\partial}{\partial r} \ln[\ell(r, \psi, R) + r - R\cos\psi] = \frac{1}{\ell(r, \psi, R)}$$
(A.9)

Q.E.D.

#### **Appendix**

## Proofs of the Radial Integrals of Poisson, Extended Hotine, and Extended Stokes Kernels

This section provides the proof of analytical solutions for the radial integral of Poisson, extended Hotine, and extended Stokes kernels given in Eqs. (34), (38), and (42), respectively. The solutions for the radially integrated Poisson and extended Hotine kernels are presented in two equivalent forms (for inverse hyperbolic tangent and natural logarithm functions), and each of them can be applied to compute the integrals numerically. To begin with, we introduce two lemmas that relate these two equivalent solutions, and are used through mathematical derivations of radial integrals of kernels.

**Lemma 1** The first expression, used to define the relation between two closed analytical solutions for the radially integrated Poisson and (extended) Hotine kernels, reads.

$$\tanh^{-1}\left[\frac{r-R\cos\psi}{\ell(r,\psi,R)}\right] = \ln\left[\ell(r,\psi,R) + r - R\cos\psi\right] + \ln\left(R\sin\psi\right)$$

**Proof** The relation between inverse hyperbolic tangent and natural logarithm is defined by.

$$\tanh^{-1} x = \frac{1}{2} \ln \frac{1+x}{1-x} = \frac{1}{2} \ln \frac{(1+x)^2}{1-x^2}$$
(A.1)

By taking into consideration the following substitution (see Lemma 1)

$$x = \frac{r - R\cos\psi}{\ell(r, \psi, R)} \tag{A.2}$$

and applying further simplifications, we get



$$\tanh^{-1} \left[ \frac{r - R\cos\psi}{\ell(r, \psi, R)} \right] = \frac{1}{2} \ln \left[ \frac{\ell(r, \psi, R) + r - R\cos\psi}{R\sin\psi} \right]^{2}$$

$$= \ln \left( \ell(r, \psi, R) + r - R\cos\psi \right) + \ln \left( R\sin\psi \right) \cdot O.E.D. \tag{A.3}$$

**Lemma 2** The second expression, applied again to define the relation between two closed analytical solutions for the radially integrated Poisson and (extended) Hotine kernels, is given by.

$$\tanh^{-1}\left[\frac{R-r\cos\psi}{\ell(r,\psi,R)}\right] = \ln\left[\frac{\ell(r,\psi,R)}{r} + \frac{R}{r} - \cos\psi\right] - \ln\left(\sin\psi\right)$$

**Proof:** The functional relation in Lemma 2 is verified by considering the following substitution.

$$x = \frac{R - r\cos\psi}{\ell(r, \psi, R)} \tag{A.4}$$

Inserting from Eq. (A.4) to Eq. (A.1), we get

$$\tanh^{-1}\left[\frac{R-r\cos\psi}{\ell(r,\psi,R)}\right] = \frac{1}{2}\ln\left[\frac{\ell(r,\psi,R) + R - r\cos\psi}{r\sin\psi}\right]^2 = \ln\left(\frac{\ell(r,\psi,R)}{r} + \frac{R}{r} - \cos\psi\right) + \ln(\sin\psi). \text{ Q.E.D.}$$
(A.5)

## **Proof of the Radially Integrated Extended Hotine Kernel**

The extended Hotine kernel in Eq. (36) was initially rewritten into the form consisting of three terms to find the solution for its radial integral; see Eq. (38). In this way, each term was integrated separately, and individual results were summed up and further simplified. In the following lemmas, the analytical solutions for the radial integral of these terms are derived in detail.

**Lemma 3** We begin with the proof of two equivalent solutions for the radial integral of the first term in Eq. (38). Hence, we write.

$$\int \frac{\mathrm{d}r}{\ell(r, \psi, R)} = \ln[\ell(r, \psi, R) + r - R\cos\psi] + C = \tanh^{-1} \left[ \frac{r - R\cos\psi}{\ell(r, \psi, R)} \right] + C$$

**Proof:** Let us rewrite the radial integral in Lamma 3 in the following complete square form:

$$\int \frac{dr}{\ell(r,\psi,R)} = \int \frac{dr}{\sqrt{(r - R\cos\psi)^2 + R^2 - R^2\cos^2\psi}} = \int \frac{dr}{R\sin\psi\sqrt{\left(\frac{r - R\cos\psi}{R\sin\psi}\right)^2 + 1}}$$
(A.10)

Introducing the following substitution including its derivative

$$t = \frac{r - R\cos\psi}{R\sin\psi}$$
 and  $dt = \frac{dr}{R\sin\psi}$  (A.11)



and inserting it to Eq. (A.10), the following standard integral is obtained

$$\int \frac{\mathrm{d}t}{\sqrt{t^2 + 1}} = \ln\left(\sqrt{t^2 + 1} - t\right) \tag{A.12}$$

Substitution from Eq. (A.11) to Eq. (A.12) then yields

$$\ln\left[\sqrt{\left(\frac{r - R\cos\psi}{R\sin\psi}\right)^2 + 1} - \frac{r - R\cos\psi}{R\sin\psi}\right] = \ln[\ell(r, \psi, R) + r - R\cos\psi] - \ln R\sin\psi$$
(A.13)

The expression in Eq. (A.13) provides the first solution for the first term in Eq. (38). According to Lemma 1, the second solution is found to be

$$\ln \left[ \sqrt{\left( \frac{r - R \cos \psi}{R \sin \psi} \right)^2 + 1} - \frac{r - R \cos \psi}{R \sin \psi} \right] = \tanh^{-1} \left[ \frac{r - R \cos \psi}{\ell(r, \psi, R)} \right]$$

**Lemma 4** The equivalent solutions for the radial integral of the second term in Eq. (38) read.

$$\begin{split} \int \ln[\ell(r,\psi,\mathbf{R}) + \mathbf{R} - r \mathrm{cos}\psi] \mathrm{d}r &= r \ln[\ell(r,\psi,\mathbf{R}) + \mathbf{R} - r \mathrm{cos}\psi] + \mathrm{R} \ln[\ell(r,\psi,\mathbf{R}) + r - \mathrm{Rcos}\psi] - r + \mathrm{C} \\ &= r \mathrm{tanh}^{-1} \left[ \frac{r - \mathrm{Rcos}\psi}{\ell(r,\psi,\mathbf{R})} \right] - \mathrm{Rtanh}^{-1} \left[ \frac{r - \mathrm{Rcos}\psi}{\ell(r,\psi,\mathbf{R})} \right] - r + \mathrm{C} \end{split}$$

**Proof:** The radial derivative of the first solution in Lemma 4 is found in the following form.

$$\begin{split} &\frac{\partial}{\partial r} \{r \ln \left[ \ell(r, \psi, R) + R - r \cos \psi \right] + R \frac{\partial}{\partial r} \{\ln \left[ \ell(r, \psi, R) + r - R \cos \psi \right] \} - \frac{\partial r}{\partial r} \\ &= \ln \left[ \ell(r, \psi, R) + R - r \cos \psi \right] + \frac{r}{\ell(r, \psi, R) + R - r \cos \psi} \left[ \frac{r - R \cos \psi}{\ell(r, \psi, R)} - \cos \psi \right] \\ &+ \frac{R}{\ell(r, \psi, R) + r - R \cos \psi} \left[ \frac{r - R \cos \psi}{\ell(r, \psi, R)} + 1 \right] - 1 \\ &= \ln \left[ \ell(r, \psi, R) + R - r \cos \psi \right] \end{split} \tag{A.14}$$

As seen in Eq. (A.14), the primitive function is obtained simply by taking its radial derivative. The radial derivative of the second solution in Lemma 4 yields the same result.

Solving the third integral is straightforward. We first consider that

$$t = r(1 - \cos\psi) \text{ and } dt = (1 - \cos\psi) dr \tag{A.15}$$

then solve the radial integral for the substitution in Eq. (A.15) and insert the result back to the solution in Eq. (A.14). The procedure yields

$$\int \ln[r(1-\cos\psi)]dr = \frac{1}{(1-\cos\psi)} \int \ln t dt = \frac{1}{(1-\cos\psi)} t(\ln t - 1) = r\{\ln[r(1-\cos\psi)] - 1\}$$
(A.16)



**Proposition 2:** According to Eq. (38), the closed analytical solutions of the radially integrated extended Hotine kernel read.

$$\int H(r, \psi, R) dr = R \ln[\ell(r, \psi, R) + r - R \cos \psi] - r \ln[\ell(r, \psi, R) + R - r \cos \psi]$$
$$+ r + r \{ \ln[r(1 - \cos \psi)] - 1 \} + C$$

and

$$\int \mathbf{H}(r, \psi, \mathbf{R}) \mathrm{d}r = \mathbf{R} \mathrm{tanh}^{-1} \left[ \frac{r - \mathbf{R} \mathrm{cos} \psi}{\ell(r, \psi, \mathbf{R})} \right] - r \mathrm{tanh}^{-1} \left[ \frac{r - \mathbf{R} \mathrm{cos} \psi}{\ell(r, \psi, \mathbf{R})} \right] + r + r \{ \ln[r(1 - \mathrm{cos} \psi)] - 1 \} + \mathbf{C} \mathrm{tanh}^{-1} \left[ \frac{r - \mathbf{R} \mathrm{cos} \psi}{\ell(r, \psi, \mathbf{R})} \right] + r + r \{ \ln[r(1 - \mathrm{cos} \psi)] - 1 \} + \mathbf{C} \mathrm{tanh}^{-1} \left[ \frac{r - \mathbf{R} \mathrm{cos} \psi}{\ell(r, \psi, \mathbf{R})} \right] + r + r \{ \ln[r(1 - \mathrm{cos} \psi)] - 1 \} + \mathbf{C} \mathrm{tanh}^{-1} \left[ \frac{r - \mathbf{R} \mathrm{cos} \psi}{\ell(r, \psi, \mathbf{R})} \right] + r + r \{ \ln[r(1 - \mathrm{cos} \psi)] - 1 \} + \mathbf{C} \mathrm{tanh}^{-1} \left[ \frac{r - \mathbf{R} \mathrm{cos} \psi}{\ell(r, \psi, \mathbf{R})} \right] + r + r \{ \ln[r(1 - \mathrm{cos} \psi)] - 1 \} + \mathbf{C} \mathrm{tanh}^{-1} \left[ \frac{r - \mathbf{R} \mathrm{cos} \psi}{\ell(r, \psi, \mathbf{R})} \right] + r + r \{ \ln[r(1 - \mathrm{cos} \psi)] - 1 \} + \mathbf{C} \mathrm{tanh}^{-1} \left[ \frac{r - \mathbf{R} \mathrm{cos} \psi}{\ell(r, \psi, \mathbf{R})} \right] + r + r \{ \ln[r(1 - \mathrm{cos} \psi)] - 1 \} + \mathbf{C} \mathrm{tanh}^{-1} \left[ \frac{r - \mathbf{R} \mathrm{cos} \psi}{\ell(r, \psi, \mathbf{R})} \right] + r + r \{ \ln[r(1 - \mathrm{cos} \psi)] - 1 \} + \mathbf{C} \mathrm{tanh}^{-1} \left[ \frac{r - \mathbf{R} \mathrm{cos} \psi}{\ell(r, \psi, \mathbf{R})} \right] + r + r \{ \ln[r(1 - \mathrm{cos} \psi)] - 1 \} + \mathbf{C} \mathrm{tanh}^{-1} \left[ \frac{r - \mathbf{R} \mathrm{cos} \psi}{\ell(r, \psi, \mathbf{R})} \right] + r + r \{ \ln[r(1 - \mathrm{cos} \psi)] - 1 \} + \mathbf{C} \mathrm{tanh}^{-1} \left[ \frac{r - \mathbf{R} \mathrm{cos} \psi}{\ell(r, \psi, \mathbf{R})} \right] + r + r \{ \ln[r(1 - \mathrm{cos} \psi)] - 1 \} + r \}$$

**Proof:** The radial integral of the extended Hotine kernel in Eq. (38) reads.

$$\int H(r, \psi, \mathbf{R}) dr = \int \frac{2\mathbf{R}}{\ell(r, \psi, \mathbf{R})} dr - \int \ln[\ell(r, \psi, \mathbf{R}) + \mathbf{R} - r\cos\psi] dr + \int \ln[r(1 - \cos\psi)] dr + \mathbf{C}$$
(A.17)

The solution of the first and second integrals in Eq. (A.17) is given in Lemmas 1 and 2, respectively. The solution of the third integral is found in Eq. (A.16). Proposition 2 is thus verified.

#### **Proof of the Radially Integrated Extended Stokes Kernel**

The extended Stokes kernel in Eq. (40) was initially rewritten into the form consisting of five terms to find the solution for its radial integral; see Eq. (42). The first term of the extended Stokes kernel is the same as that of the extended Hotine kernel for which the solution was found in Eq. (A.8). Radial integrals of the second and fourth terms have standard solutions. Consequently, the proof is given only for the radial integral of the third and fifth terms.

To solve the radial integral of the third term, we must find solutions for some integrals first and thereafter use them to obtain the radial integral of the third term.

From Eq. (40), we write the radially integrated Stokes kernel in the following form

$$\int S(r,\psi,R)dr = 2R \int \frac{1}{\ell(r,\psi,R)}dr + R \int r^{-1}dr - 3R \int \frac{\ell(r,\psi,R)}{r^2}dr - 5R^2\cos\psi \int r^{-2}dr - 3R^2\cos\psi \int r^{-2}\ln\left[\frac{\ell(r,\psi,R) + r - R\cos\psi}{2r}\right]dr$$
(A.18)

**Lemma 5** We introduce the following radial integral and its two equivalent solutions in terms of natural logarithm and inverse hyperbolic tangent functions.

$$\int \frac{1}{r\ell(r,\psi,R)} dr = -\frac{1}{R} \ln\left(\frac{l}{r} + \frac{R}{r} - \cos\psi\right) + C = -\frac{1}{R} \tanh^{-1} \left[\frac{R - r\cos\psi}{\ell(r,\psi,R)}\right] + C$$

**Proof:** To provide proof for the first integral solution in Lemma 1, we consider the following substitution and its radial derivative.



$$t = \frac{1}{r}, \text{ and } dt = -\frac{dr}{r^2} \tag{A.19}$$

Substituting from Eq. (A.19) to the radial integral and writing the result in the form of complete square, we arrive at

$$\int \frac{1}{r\ell(r,\psi,R)} dr = \int \frac{1}{\sqrt{(R t - \cos\psi)^2 - \cos^2\psi + 1}} dr$$
(A.20)

To change the integral in Eq. (A.20) to a standard form for which the solution is given, we apply the following substitution and its radial derivative

$$w = \frac{R t - \cos \psi}{\sin \psi} \text{ and } dw = \frac{R dt}{\sin \psi}$$
 (A.21)

Substitution from Eq. (A.21) to Eq. (A.20) yields

$$\int \frac{1}{\sqrt{(R t - \cos \psi)^2 - \cos^2 \psi + 1}} dr = \frac{1}{R} \int \frac{\sin \psi}{\sqrt{w^2 + 1}} dw = \frac{1}{R} \ln \left( \sqrt{w^2 + 1} + 1 \right) + C$$
(A.22)

Combining Eqs. (A.19)–(A.22), we arrive at

$$\int \frac{1}{\sqrt{(Rt - \cos\psi)^2 - \cos^2\psi + 1}} dr = -\frac{1}{R} \ln\left(\frac{\ell(r, \psi, R)}{r} + \frac{R}{r} - \cos\psi\right) + C$$
$$= -\frac{1}{R} \tanh^{-1} \left[\frac{R - r\cos\psi}{\ell(r, \psi, R)}\right] + C \tag{A.23}$$

The result in Eq. (A.23) is the first solution, while the second solution is found by applying Lemma 2.

**Lemma 6** We further write the solution for the radial integral of the following radial derivative.

$$\int \frac{\partial}{\partial r} \frac{\ell(r, \psi, \mathbf{R})}{r} dr = \tanh^{-1} \left[ \frac{r - \mathbf{R} \cos \psi}{\ell(r, \psi, \mathbf{R})} \right] + \cos \psi \tanh^{-1} \left[ \frac{\mathbf{R} - r \cos \psi}{\ell(r, \psi, \mathbf{R})} \right] + \mathbf{C}$$

**Proof:** The radial integral on the right-hand side of Lemma 6 is separated into two integrals, i.e.,

$$\int \frac{\partial}{\partial r} \frac{\ell(r, \psi, R)}{r} dr = \int \frac{1}{\ell(r, \psi, R)} dr - R\cos\psi \int \frac{1}{r\ell(r, \psi, R)} dr$$
(A.24)

The first integral on the right-hand side of Eq. (A.24) is given in Lemma 3. Based on Lemma 4, Lemma 6 is verified.

**Lemma 7** We now introduce the following integral and its analytical solution.



$$\int \frac{\ell(r, \psi, \mathbf{R})}{r^2} dr = -\frac{\ell(r, \psi, \mathbf{R})}{r} + \tanh^{-1} \left[ \frac{r - \mathbf{R} \cos \psi}{\ell(r, \psi, \mathbf{R})} \right] + \cos \psi \tanh^{-1} \left[ \frac{\mathbf{R} - r \cos \psi}{\ell(r, \psi, \mathbf{R})} \right] + \mathbf{C}$$

**Proof:** Let us use the integration by part for the following two terms.

$$u(r, \psi, \mathbf{R}) = \ell(r, \psi, \mathbf{R}), \text{ and } dv = \frac{dr}{r^2}$$
 (A.25)

Inserting from Eq. (A.25) back to Lemma 7, we get

$$\int \frac{\ell(r, \psi, R)}{r^2} dr = -\frac{\ell(r, \psi, R)}{r} + \int \frac{\partial \ell(r, \psi, R)}{r \partial r} dr$$
(A.26)

Based on Lemma 6, Lemma 7 is verified.

**Lemma 8** The equivalent two solutions of the radial integral of the function  $r^{-2}\ell^{-1}$  read.

$$\int \frac{\mathrm{d}r}{r^2 \ell(r, \psi, \mathbf{R})} = -\frac{1}{r \, \mathbf{R}^2} + \frac{\cos \psi}{\mathbf{R}^2} \ln \left( \frac{1}{r} + \frac{\mathbf{R}}{r} - \cos \psi \right) + \mathbf{C} = -\frac{1}{r \, \mathbf{R}^2} - \frac{\cos \psi}{\mathbf{R}^2} \tanh^{-1} \left[ \frac{\mathbf{R} - r \cos \psi}{\ell(r, \psi, \mathbf{R})} \right] + \mathbf{C}$$

**Proof:** For  $t = r^{-1}$  we have  $dt = -r^{-2}dr$ . Applying this substitution to Lemma 8, we get.

$$\int \frac{\mathrm{d}r}{r^2 \ell(r, \psi, \mathbf{R})} = -\int \frac{t \, \mathrm{d}t}{\sqrt{\mathbf{R}^2 t^2 - 2\mathbf{R} \, t \cos \psi + 1}} \tag{A.27}$$

To find the solution of Eq. (A.27), we further introduce the following substitution

$$t = \frac{1}{2R^2} \left( 2R^2 t - 2R\cos\psi \right) + \frac{\cos\psi}{R}$$
 (A.28)

for the numerator of the integrant so that we can split the integral into two parts with simple solutions.

Inserting from Eq. (A.28) back to Eq. (A.27), we arrive at

$$\int \frac{t \, dt}{\sqrt{R^2 t^2 - 2R \, t \cos \psi + 1}} = \frac{1}{R} \int \frac{Rt - \cos \psi}{\sqrt{R^2 t^2 - 2Rt \cos \psi + 1}} dt + \frac{\cos \psi}{R} \int \frac{dt}{\sqrt{R^2 t^2 - 2Rt \cos \psi + 1}}$$
(A.29)

The solution of the first integral in Eq. (A.29) is given by

$$\frac{1}{R} \int \frac{Rt - \cos\psi}{\sqrt{R^2 t^2 - 2Rt\cos\psi + 1}} dt = \frac{1}{R} \sqrt{R^2 t^2 - 2Rt\cos\psi + 1} = \frac{1}{rR^2}$$
 (A.30)

The solution of the second integral in Eq. (A.29) is simple after completing the square, i.e.,

$$\frac{\cos\psi}{R} \int \frac{dt}{\sqrt{R^2 t^2 - 2Rt \cos\psi + 1}} = \frac{\cos\psi}{R^2} \ln\left(\frac{1}{r} + \frac{R}{r} - \cos\psi\right) + C \tag{A.31}$$



The proof of the logarithmic solution in Lemma 8 is obtained by inserting from Eqs. (A.30) and (A.31) back to Eq. (A.29), while the proof for the second solution is found by applying Lemma 2.

**Lemma 9** The fifth radial integral in Eq. (A.18) has the following closed analytical solution.

$$\int r^{-2} \ln \left[ \frac{\ell(r,\psi,R) + r - R\cos\psi}{2r} \right] dr = -\frac{1}{r} \ln \left[ \frac{\ell(r,\psi,R) + r - R\cos\psi}{2r} \right] - \frac{1}{R} \tanh^{-1} \left[ \frac{R - r\cos\psi}{\ell(r,\psi,R)} \right] + \frac{1}{r} \ln \left[ \frac{R - r\cos\psi}{2r} \right] + \frac{1}{r} \ln \left[ \frac{R - r\cos\psi}{2r$$

**Proof:** The integral in Lemma 9 is first simplified as follows.

$$\int r^{-2} \ln \left[ \frac{\ell(r, \psi, R) + r - R \cos \psi}{2r} \right] dr = \int r^{-2} [\ell(r, \psi, R) + r - R \cos \psi] dr - \int r^{-2} \ln (2r) dr$$
(A.32)

To find the solution for the first integral on the right-hand side of Eq. (A.32), we introduce

$$u = \ln[\ell(r, \psi, R) + r - R\cos\psi] \text{ and } dv = \frac{dr}{r^2}$$
(A.33)

Inserting from Eq. (A.33) to Eq. (A.32), and applying the integration by part, we get

$$\int r^{-2} \ln \left[ \ell(r, \psi, R) + r - R \cos \psi \right] dr = -\frac{1}{r} \ln \left[ \ell(r, \psi, R) + r - R \cos \psi \right]$$

$$- \int \frac{\partial}{\partial r} \ln \left[ \ell(r, \psi, R) + r - R \cos \psi \right] r^{-1} dr$$
(A.34)

Based on Eq. (A.9), we see that the integral term on the right-hand side of Eq. (A.34) was provided in Lemma 8, hence

$$\int r^{-2} \ln \left[ \ell(r, \psi, R) + r - R \cos \psi \right] dr = -\frac{1}{r} \ln \left[ \ell(r, \psi, R) + r - R \cos \psi \right] - \frac{1}{R} \tanh^{-1} \left[ \frac{R - r \cos \psi}{\ell(r, \psi, R)} \right] + C \tag{A.35}$$

The solution of the second integral on the right-hand side of Eq. (A.32) is found by integrating by part, hence

$$\int r^{-2} \ln 2r dr = -r^{-1} \ln 2r + \int \frac{1}{r} dr + C = -\frac{\ln 2r + 1}{r} + C$$
 (A.36)

Substitution from Eqs. (A.35) and (A.36) to Eq. (A.32) yields



$$\int r^{-2} \ln \left[ \frac{\ell(r, \psi, R) + r - R \cos \psi}{2r} \right] dr = \int r^{-2} [\ell(r, \psi, R) + r - R \cos \psi] dr - \int r^{-2} \ln (2r) dr$$

$$= -\frac{1}{r} \ln \left[ \ell(r, \psi, R) + r - R \cos \psi \right] - \frac{1}{R} \tanh^{-1} \left[ \frac{R - r \cos \psi}{\ell(r, \psi, R)} \right] + \frac{\ln 2r + 1}{r} + C$$

$$= -\frac{1}{r} \ln \left[ \ell(r, \psi, R) + r - R \cos \psi \right] + \frac{\ln 2r}{r} - \frac{1}{R} \tanh^{-1} \left[ \frac{R - r \cos \psi}{\ell(r, \psi, R)} \right] + \frac{1}{r} + C$$

$$= -\frac{1}{r} \ln \left[ \frac{\ell(r, \psi, R) + r - R \cos \psi}{2r} \right] - \frac{1}{R} \tanh^{-1} \left[ \frac{R - r \cos \psi}{\ell(r, \psi, R)} \right] + \frac{1}{r} + C$$

$$(A.37)$$

**Proposition 3:** The radial integral of the extended Stokes kernel is given by.

$$f S(r, \psi, R) dr = 2R \tanh^{-1} \left[ \frac{r - R \cos \psi}{\ell(r, \psi, R)} \right] + R \ln(r)$$

$$+3R \left\{ \frac{\ell(r, \psi, R)}{r} - \tanh^{-1} \left[ \frac{r - R \cos \psi}{\ell(r, \psi, R)} \right] - \cos \psi \tanh^{-1} \left[ \frac{R - r \cos \psi}{\ell(r, \psi, R)} \right] \right\}$$

$$+5R^{2} \cos \psi \frac{1}{r} + 3R^{2} \cos \psi \left\{ \frac{1}{r} \ln \left[ \frac{\ell(r, \psi, R) + r - R \cos \psi}{2r} \right] + \frac{1}{R} \tanh^{-1} \left[ \frac{R - r \cos \psi}{\ell(r, \psi, R)} \right] - \frac{1}{r} \right\}$$
(A.38)

**Proof** Taking into consideration the following well-known integral solutions.

$$\int r^{-1}dr = \ln r + C \tag{A.39}$$

and

$$\int r^{-2}dr = -r^{-1} + C \tag{A.40}$$

and applying Lemmas 3, 6, and 9 in Eq. (A.18), Proposition 3 is verified.

**Acknowledgements** The research was conducted during the research stay of Robert Tenzer at the University of West Bohemia in Pilsen, Czech Republic. Pavel Novák was supported by the project 23-07031S of the Czech Science Foundation. We appreciate valuable comments and suggestions of the anonymous reviewers, which helped to improve the quality of the manuscript.

Funding Open access funding provided by The Hong Kong Polytechnic University.

#### **Declarations**

**Conflict of interest** There is no conflict of interests.

Open Access This article is licensed under a Creative Commons Attribution 4.0 International License, which permits use, sharing, adaptation, distribution and reproduction in any medium or format, as long as you give appropriate credit to the original author(s) and the source, provide a link to the Creative Commons licence, and indicate if changes were made. The images or other third party material in this article are included in the article's Creative Commons licence, unless indicated otherwise in a credit line to the material. If material is not included in the article's Creative Commons licence and your intended use is not permitted by statutory regulation or exceeds the permitted use, you will need to obtain permission directly from the copyright holder. To view a copy of this licence, visit http://creativecommons.org/licenses/by/4.0/.



#### References

- Bayoud FA, Sideris MG (2003) Two different methodologies for geoid determination from surface and airborne gravity data. Geophys J Int 155:914–922
- Bjerhammar A (1975) Discrete approaches to the solution of the boundary value problem in physical geodesy. Bol Geod E Sd Aft XXXIV 2:185–240
- Bjerhammar A (1985) On a Relativistic Geodesy. Bull Géodésique 59:207–220
- Bjerhammar A (1986) Relativistic geodesy. NOAA Technical Report, NOS 118 NGS 36
- Burša M, Kouba J, Kumar M, Müller A, Radej K, True SA, Vatrt V, Vojtíšková M (1999) Geoidal geopotential and world height system. Stud Geoph Geod 43:327–337
- Colombo O (1980) A world vertical network. Report 296, Department of Geodetic Science and Surveying, Ohio State University, Columbus
- Drinkwater MR, Floberghagen R, Haagmans R, Muzi D, Popescu A (2003) GOCE: ESA's first Earth Explorer Core mission. In: Beutler G, Drinkwater MR, Rummel R, Von Steiger R (eds) Earth Gravity Field from Space — From Sensors to Earth Sciences. Space Sciences Series of ISSI, vol 17. Springer, Dordrecht
- Floberghagen R, Fehringer M, Lamarre D, Muzi D, Frommknecht B, Steiger C, Piñeiro J, da Costa A (2011) Mission design, operation and exploitation of the gravity field and steady-state ocean circulation explorer mission. J Geod 85(11):749–758
- Förste C, Bruinsma SL, Abrikosov O, Lemoine JM, Marty JC, Flechtner F, Balmino G, Barthelmes F, Biancale R (2014) EIGEN-6C4 The latest combined global gravity field model including GOCE data up to degree and order 2190 of GFZ Potsdam and GRGS Toulouse. GFZ Data Services Tapley BD, Bettadpur S, Watkins M
- Gradshteyn IS, Ryzhik IM (2007) Table of Integrals, Series, and Product, 7th edn. Academic Press, Elsevier Inc.
- Grafarend EW (2001) The spherical horizontal and spherical vertical boundary value problem vertical deflections and geoidal undulations the completed Meissl diagram. J Geod 75(7–8):363–390
- Hager B, Richards M (1989) Long-wavelength variations in Earth's geoid: physical models and dynamical implications. Philos Trans R Soc Math Phys Sci 328:309–327
- Hager BH, Clayton RW, Richards MA, Comer RP, Dziewonski AM (1985) Lower mantle heterogeneity, dynamic topography and the geoid. Nature 313:541–545
- Heck B (1997) Formulation and linearization of boundary value problems: from observables to a mathematical model. In geodetic boundary value problems in view of the one centimeter geoid. Lect Notes Earth Sci 65:119–160
- Heck B (1991) On the linearized boundary value problem of physical geodesy, Department of Geodetic Science and Survey, The Ohio State University, Rep 407, Columbus, Ohio
- Heiskanen W, Moritz H (1967) Physical Geodesy. WH Freeman and Co., San Francisco-London
- Helmert FR (1880) Die mathematischen und physicalischen Theorien der hoheren Geodasie. Teubner, Leipzip (in German)
- Ji Y, Tenzer R, Tang H, Sun W (2023) Coseismic gravitational curvatures changes in a spherical symmetric earth model. Phys Earth Planet Inter 338:107013
- Kellogg OD (1967) Foundations of potential theory, 1st edn. Springer, Verlag
- Kopeikin S, Vlasov I, Han W (2018) Normal gravity field in relativistic geodesy. Phys Rev 97(4):045020
- Mai E (2013) Time, atomic clocks, and relativistic geodesy. Germany, Deutsche Geodätische Kommission (DGK), München
- Martinec Z (2003) Green's function solution to spherical gradiometric boundary-value problems. J Geod 77:41–49
- Martinec Z (1998) Boundary-value problems for gravimetric determination of a precise geoid Lecture Notes in Earth Sciences, vol 73. Springer-Verlag, Heidelberg
- McKenzie DP (1967) Some remarks on heat flow and gravity anomalies. J Geophys Res 72(24):6261–6273
- McKenzie DP, Fairhead D (1997) Estimates of the effective elastic thickness of the continental lithosphere from Bouguer and free-air gravity anomalies. J Geophys Res 102:27523–27552
- Mehlstäubler TE, Grosche G, Lisdat C, Schmidt PO, Denker H (2018) Atomic clocks for geodesy. Rep Prog Phys 81(6):064401
- Meissl P (1971) A study of covariance functions related to the earth's disturbing potential. Report No. 151, The Ohio State University, Columbus, Ohio
- Moritz H (2000) Geodetic reference system 1980. J Geod 74:128162
- Panet I, Pajot-Métivier G, Greff-Lefftz M, Métivier L, Diament M, Mandea M (2014) Mapping the mass distribution of Earth's mantle using satellite-derived gravity gradients. Nat Geosci 7(2):131–135



- Phillips RJ, Lambeck K (1980) Gravity fields of the terrestrial planets: long-wavelength anomalies and tectonics. Rev Geophys Sp Phys 18:27–76
- Puetzfeld D, Lämmerzahl C, Puetzfeld D, Lämmerzahl C (2019) Relativistic geodesy, vol 196. Springer International Publishing, Cham
- Rummel R, Van Gelderen M (1992) Spectral analysis of the full gravity tensor. Geophys J Int 111(1):159–169
- Shen W, Ning J, Liu J, Liu J, Chao D (2011) Determination of the geopotential and orthometric height based on frequency shift equation. Nat Sci 3(5):388–396
- Shen W, Sun X, Cai C, Wu K, Shen Z (2019) Geopotential determination based on a direct clock comparison using two-way satellite time and frequency transfer. Terr Atmos Ocean Sci 30(1):21–31
- Sjöberg LE (2006) A refined conversion from normal height to orthometric height. Stud Geophys Geod 50:595-606
- Šprlák M, Novák P (2015) Integral formulas for computing a third-order gravitational tensor from volumetric mass density, disturbing gravitational potential, gravity anomaly and gravity disturbance. J Geodesy 89:141–157
- Šprlák M, Novák P (2016) Spherical gravitational curvature boundary-value problem. J Geodesy 90:727–739
- Šprlák M, Novák P (2017) Spherical integral transforms of second-order gravitational tensor com-ponents onto third-order gravitational tensor components. J Geodesy 91:167–194
- Steinberger B (2000) Slabs in the lower mantle Results of dynamic modelling compared with tomographic images and the geoid. Phys Earth Planet Inter 118:241–257
- Stokes GG (1849) On the variation of gravity on the surface of the Earth. Trans Cambridge Phil Soc 8:672-695
- Tenzer R, Chen W (2019) Mantle and sub-lithosphere mantle gravity maps from the LITHO1.0 global lithospheric model. Earth Sci Rev 194:38–56
- Tenzer R, Vaníček P, Santos M, Featherstone WE, Kuhn M (2005) The rigorous determination of orthometric heights. J Geod 79(1–3):82–92
- Tenzer R, Novák P, Moore P, Kuhn M, Vaníček P (2006) Explicit formula for the geoid-quasigeoid separation. Stud Geophys Geod 50:607–618
- Tenzer R, Gladkikh V, Vajda P, Novák P (2012) Spatial and spectral analysis of refined gravity data for modelling the crust-mantle interface and mantle-lithosphere structure. Surv Geophys 33(5):817–839
- Tenzer R, Hamayun K, Vajda P (2009) A global correlation of the step-wise consolidated crust-stripped gravity field quantities with the topography, bathymetry, and the CRUST2.0 Moho boundary. Contrib Geophys Geod 39(2):133–147
- Tenzer R, Chen W, Tsoulis D, Bagherbandi M, Sjöberg LE, Novák P, Jin S (2015) Analysis of the refined CRUST1.0 crustal model and its gravity field. Surv Geophys 36(1):139–165
- Vajda P, Vaníček P, Novák P, Tenzer R, Ellmann A (2007) Secondary indirect effects in gravity anomaly data inversion or interpretation. J Geophys Res (Solid Earth) 112:B06411
- van Gelderen M, Koop R (1997) The use of degree variances in satellite gradiometry. J Geod 71:337–343
- Vaníček P, Tenzer R, Sjöberg LE, Martinec Z, Featherstone WE (2005) New views of the spherical Bouguer gravity anomaly. Geophys J Int 159:460–472
- Vaníček P, Janák J, Huang J (2001) Mean vertical gradient of gravity. In: Sideris MG (eds.). Gravity Geoid and Geodynamics 2000. International Association of Geodesy Symposia vol 123. Springer. Berlin
- Vermeer M (1983) Chronometric levelling. Reports of the Finnish Geodetic Institute Vol 83, No 2, Geodeettinen Laitos, Geodetiska Institutet, ISSN 0355–1962
- Watts AB, Talwani M (1974) Gravity anomalies seaward of deep-sea trenches and their tectonic implications. Geophys J Int 36(1):57–90

**Publisher's Note** Springer Nature remains neutral with regard to jurisdictional claims in published maps and institutional affiliations.



#### **Authors and Affiliations**

## Robert Tenzer<sup>1</sup> • Pavel Novák<sup>2</sup> • Mehdi Eshagh<sup>3</sup>

- Robert Tenzer robert.tenzer@polyu.edu.hk
- Department of Land Surveying and Geo-Informatics, The Hong Kong Polytechnic University, 181 Chatham Road South, Kowloon, Hong Kong
- NTIS New Technologies for the Information Society, Faculty of Applied Sciences, University of West Bohemia, Univerzitní 22, Plzen, Czech Republic
- Division of Meteorology-Forecast and Observations, Swedish Meteorological and Hydrological Institute, Norrköping, Sweden

